

CARBON SUPPORTED PLATINUM-PALLADIUM CATALYSTS FOR
METHANOL AND ETHANOL OXIDATION REACTIONS

A THESIS SUBMITTED TO
THE GRADUATE SCHOOL OF NATURAL AND APPLIED SCIENCES
OF
MIDDLE EAST TECHNICAL UNIVERSITY

BY

ZAFER ÖZTÜRK

IN PARTIAL FULFILLMENT OF THE REQUIREMENTS
FOR
THE DEGREE OF MASTER OF SCIENCE
IN
CHEMISTRY

FEBRUARY 2011

Approval of the thesis:

**CARBON SUPPORTED PLATINUM-PALLADIUM CATALYSTS FOR
METHANOL AND ETHANOL OXIDATION REACTIONS**

submitted by **ZAFER ÖZTÜRK** in partial fulfillment of the requirements for the degree of **Master of Science in Chemistry Department, Middle East Technical University** by,

Prof. Dr. Canan Özgen
Dean, Graduate School of **Natural and Applied Sciences** _____

Prof. Dr. İlker Özkan
Head of Department, **Chemistry** _____

Prof. Dr. Gülsün Gökağaç
Supervisor, **Chemistry Department, METU** _____

Examining Committee Members:

Prof. Dr. İnci Eroğlu
Chemical Engineering Dept., METU _____

Prof. Dr. Gülsün Gökağaç
Chemistry Dept., METU _____

Prof. Dr. Ceyhan Kayran
Chemistry Dept., METU _____

Assoc. Prof. Dr. Ayşen Yılmaz
Chemistry Dept., METU _____

Assist. Prof. Dr. Emren Nalbant Esentürk
Chemistry Dept., METU _____

Date: **11.02.2011**

I hereby declare that all information in this document has been obtained and presented in accordance with academic rules and ethical conduct. I also declare that, as required by these rules and conduct, I have fully cited and referenced all materials and results that are not original to this work.

Name, Last name: Zafer Öztürk

Signature:

ABSTRACT

CARBON SUPPORTED PLATINUM-PALLADIUM CATALYSTS FOR METHANOL AND ETHANOL OXIDATION REACTIONS

Öztürk, Zafer

M. Sc., Department of Chemistry

Supervisor: Prof. Dr. Gülsün Gökağaç

February 2011, 53 pages

In this work, two groups of carbon supported Pt-Pd catalysts have been prepared in order to investigate the effect of Pd, as a second metal, and surfactants on the catalytic activity towards methanol and ethanol oxidation reactions used in the direct methanol and ethanol fuel cells. In the first group (group a), 1-hexanethiol was used as a stabilizing agent while in the second group (group b), 1,1-dimethyl hexanethiol was utilized. Cyclic voltammetry (CV), chronoamperometry (CA), X-ray diffraction (XRD), transmission electron microscopy (TEM), energy dispersive X-ray spectroscopy (EDS) and X-ray photoelectron spectroscopy (XPS) were used in order to determine the nature of the catalysts.

The average crystalline size of the metal particles in the catalysts was explored by XRD and TEM. TEM results revealed the uniform distribution of the metal nanoparticles on carbon support with a narrow size distribution in the range of 3.0 to 3.7 nm and the average crystalline sizes of metal particles for group “b” catalysts were larger than that of group “a” catalysts which can be explained by the surfactant effect. These results were in good agreement with XRD data.

The oxidation states of platinum (Pt(0) and Pt(IV)) and palladium (Pd(0) and Pd(II)) and their ratios were investigated by XPS and for the most active catalyst, catalyst Ib, these ratios were found to be as 6.94 and 13.7, respectively.

Electrochemical activities of the catalysts towards methanol and ethanol oxidation reactions were recorded and compared with that of Pt/C and the commercial Pt (E-TEK 20 %wt) catalysts. The results indicated that the group 'b' catalyst has greater catalytic activities than that of group 'a' catalysts. Catalyst Ib comes into prominence as the most active catalyst due to its superior characteristics that it possess such as highest extent of alloying with respect to the palladium amount used, active surface area, CO-tolerance, stability and Pt (0) to Pt (IV) and Pd (0) to Pd (II) ratios.

Keywords: Direct Methanol & Ethanol Fuel Cells, Carbon Supported Platinum and Palladium Catalysts, Cyclic Voltammetry, Transmission Electron Microscopy, X-ray Photoelectron Spectroscopy.

ÖZ

METANOL VE ETANOL YÜKSELTGENME TEPKİMELERİ İÇİN KARBON DESTEKLİ PLATİN-PALADYUM KATALİZÖRLERİ

Öztürk, Zafer

Yüksek Lisans, Kimya Bölümü

Tez Yöneticisi: Prof. Dr. Gülsün Gökagaç

Şubat 2011, 53 sayfa

Bu çalışmada doğrudan metanol ve etanol yakıt hücrelerinde kullanılan metanol ve etanol yükseltgenme tepkimeleri için iki grup Pt-Pd katalizörleri hazırlanmış ve Paladyumun ve katalizörlerin hazırlanması aşamasında kullanılan sürfaktantların katalizörlerin aktiviteleri üzerindeki etkileri incelenmiştir. İlk grupta (grup a) 1-hekzantiol sürfaktant olarak kullanılırken, ikinci grupta (grup b) 1,1 dimetil hekzantiol kullanılmıştır. Dönüşümlü voltametre (CV), kronoamperometre (CA), X-ışınları kırınımı (XRD), geçirmeli elektron mikroskobu (TEM), enerji dağılım X-ışınları spektroskopisi (EDS) ve X-ışınları fotoelektron spektroskopisi (XPS) katalizörlerin doğasının tayini için kullanılmıştır.

Katalizörlerdeki ortalama metal parçacıklarının büyüklüğü X-ışınları kırınımı (XRD) ve geçirmeli elektron mikroskobu (TEM) yardımıyla incelenmiştir. TEM sonuçları metal nanoparçacıkların karbon destek üzerinde 3.0 ve 3.7 nm arasında değişen dağılımını ortaya koymuştur. Ayrıca “b” grubu katalizörlerdeki metal parçacık boyutunun “a” grubu katalizörlerine göre daha büyük olduğunu göstermiş ve sonuç sürfaktant etkisi ile açıklanmıştır. XRD verilerinin de TEM sonuçlarıyla uyum içinde olduğunu göstermiştir.

Platin (Pt(0) ve Pt(IV)) ve paladyum (Pd(0) ve Pd(II)) için oksidasyon deęerlikleri ve bunların birbirlerine oranları X-ışınları fotoelektron spektroskopu (XPS) aracılığıyla incelenmiş ve en aktif katalizör için (katalizör Ib) sırasıyla 6.94 ve 13.7 olarak bulunmuştur.

Katalizörlerin metanol ve etanol yükseltgenme tepkimelerine karşı elektrokimyasal aktiviteleri tayin edilmiş, Pt/C ve ticari Pt (E TEK 20 %wt) katalizörlerin aktiviteleri ile kıyaslanmıştır. Sonuçlar “b” grubu katalizörlerinin “a” grubu katalizörlerinden daha yüksek katalitik aktiviteye sahip olduğu göstermiştir. Katalizör Ib’nin kullanılan paladyum miktarına göre en yüksek derecede alaşım oluşturma, en yüksek aktif yüzey alanına, CO toleransına, kararlılığa ve Pt(0)/Pt(IV) ve Pd(0)/Pd(II) oranlarına sahip olmasından dolayı en aktif katalizör olduğu bulunmuştur.

Anahtar Kelimeler: Doğrudan Metanol ve Etanol Yakıt Hücreleri, Karbon Destekli Platin ve Paladyum Katalizörleri, Dönüşümlü Voltametre, Geçirmeli Elektron Mikroskopu, X-ışınları Fotoelektron Spektroskopu.

To my family...

ACKNOWLEDGEMENTS

I would like to express my deep and sincere gratitude to my advisor Prof. Dr. Gülsün Gökağaç. Her wide knowledge and her logical way of thinking have been of great value for me. Her understanding, encouraging and personal guidance have provided a good basis for the present thesis.

I wish to express my sincere appreciation to Fatih Şen for his support, answering my never ending questions and guidance to improve my skills during my study.

I gratefully thank to Selda Şen for her support, valuable ideas and motivation during my studies.

I owe many thanks to my lab partner Salih Ertan who is always ready to give a hand whenever I needed.

I truly thank to my dearest friends, Berrin Özkan, Ebru Ünel, Feriye Şenol, Meryem & Erkunt Karabulut, Okan Karl Kittelson, Rukan Koşak, Serdar Akbayrak, Salim Çalışkan, Tuğba Orhan who were with me in this challenging process, for their precious friendship.

I also would like to thank to TUBITAK (108T065) for the financial support and to METU Central Laboratory for the analysis.

Lastly, my deepest gratitude goes to my beloved parents, Güngör & Metin Öztürk, and my brother, Mevlüt Öztürk, who always supported me and believed in me. Without their encouragement and immeasurable sacrifice, I could never finish this journey.

TABLE OF CONTENTS

| | |
|--|----|
| ABSTRACT..... | iv |
| ÖZ..... | vi |
| ACKNOWLEDGEMENTS..... | ix |
| CHAPTERS..... | 1 |
| INTRODUCTION..... | 1 |
| 1.1. FUEL CELLS AND THEIR SIGNIFICANCE FOR THE ECONOMY..... | 1 |
| 1.2. THE LONG HISTORY OF FUEL CELLS..... | 2 |
| 1.3. TYPES OF FUEL CELLS..... | 7 |
| 1.4. THE DIRECT METHANOL FUEL CELLS..... | 9 |
| 1.5. THE DIRECT ETHANOL FUEL CELLS..... | 11 |
| 1.6. THE OBJECTIVE OF STUDY..... | 14 |
| EXPERIMENTAL..... | 15 |
| 2.1. SYNTHESIS OF CATALYSTS..... | 15 |
| 2.1.1. SYNTHESIS OF CATALYST Ia..... | 15 |
| 2.1.2. SYNTHESIS OF CATALYSTS IIa, IIIa, Ib, IIb, IIIb..... | 16 |
| 2.1.3. SYNTHESIS OF Pt/C (a & b)..... | 16 |
| 2.2. ELECTRODE PREPARATION..... | 17 |
| 2.3. PLATINUM & PALLADIUM CONTENT DETERMINATION..... | 17 |
| 2.4. CHARACTERIZATION TECHNIQUES..... | 17 |
| 2.4.1. CYCLIC VOLTAMMETRY (CV)..... | 17 |
| 2.4.2. CHRONOAMPEROMETRY (CA)..... | 19 |
| 2.4.3. X-RAY DIFFRACTION..... | 21 |
| 2.4.4. TRANSMISSION ELECTRON MICROSCOPY (TEM) AND ENERGY DISPERSIVE X-RAY SPECTROSCOPY (EDS)..... | 23 |
| 2.4.5. X-RAY PHOTOELECTRONSPECTROSCOPY (XPS)..... | 24 |

| | |
|--|----|
| RESULTS AND DISCUSSION | 26 |
| 3.1. X-RAY DIFFRACTION (XRD) AND TRANSMISSION ELECTRON MICROSCOPY (TEM) | 26 |
| 3.2. X-RAY PHOTOELECTRON SPECTROSCOPY | 35 |
| 3.3. CYCLIC VOLTAMMETRY AND CHRONOAMPEROMETRY | 37 |
| CONCLUSIONS..... | 49 |

LIST OF TABLES

TABLES

| | |
|--|----|
| Table 1. Types of fuel cells and their major characteristics with their fields of application areas..... | 8 |
| Table 2. Platinum complexes and surfactants used for all prepared catalysts. | 16 |
| Table 3. Peak positions, lattice parameter, atomic percent of platinum and palladium in all catalysts. | 28 |
| Table 4. Pt 4f _{7/2} and Pd 3d _{3/2} Core Binding Energies, eV, for Pt-Pd catalysts (The numbers in parentheses are the relative percent intensities of the species.). | 37 |
| Table 5. The onset and anodic peak potential, I _f /I _b ratios for all prepared catalysts in MeOH and EtOH..... | 46 |
| Table 6. The comparisons of particle size, ECSA, CSA and ECSA/CSA (% catalyst utility) for all catalysts. | 48 |

LIST OF FIGURES

FIGURES

| | |
|---|----|
| Figure 1. Grove's gas battery (1839). | 4 |
| Figure 2 Schematic representation of a DMFC | 10 |
| Figure 3. Schematic diagram of a DEFC ⁹ | 12 |
| Figure 4. Typical excitation signal for cyclic voltammetry. | 18 |
| Figure 5. A typical cyclic voltammogram displaying reduction and oxidation current peaks..... | 19 |
| Figure 6. A typical chronoamperogram. Inset is the excitation waveform ²² | 20 |
| Figure 7. The incident and scattered X-rays. | 21 |
| Figure 8. Illustration for the derivation of binding energy where E_k is the kinetic energy of the photoelectrons, E_i is the initial state and E_f is the final state ²⁷ | 25 |
| Figure 9. Dependence of fcc lattice constant (a in angstroms) on the Pt content of the Pt/C (b), catalyst Ib, catalyst IIb and catalyst IIIb..... | 27 |
| Figure 10. XRD diffraction pattern of Pt/C a (a), catalysts Ia (b), IIa (c), IIIa (d), Pt/C b (e), catalysts Ib (f), IIb (g) and IIIb (h). | 29 |
| Figure 11. Size distribution of catalyst Ia (a), IIa (b), IIIa (c), Ib (d), IIb (e) and IIIb (f)..... | 30 |
| Figure 12. A schematic representation of the formation of the group 'a' and 'b' Pt-Pd nanoparticles. | 31 |
| Figure 13. Transmission electron micrograph of catalyst Ib (a) and IIIa (b). | 33 |
| Figure 14. a) Transmission electron micrograph and b) EDS results for the spectrum 1 region of catalyst Ib..... | 34 |
| Figure 15. Pt 4f electron spectra of catalyst Ia (a), IIa (b), IIIa (c), Ib (d), IIb (e) and IIIb (f)..... | 35 |
| Figure 16. Pd 3d _{3/2} electron spectra of catalyst Ia (a), Ib (b), IIa (c)..... | 36 |

| | |
|--|----|
| Figure 17. Cyclic voltammogram of catalyst Ib in 0.1 M HClO ₄ . | 38 |
| Figure 18. Cyclic voltammogram of catalyst Ib in 0.1 M HClO ₄ + 0.5 M CH ₃ OH at room temperature with a scan rate of 50 mV/s. | 38 |
| Figure 19. Cyclic voltammogram of catalyst Ib in 0.1 M HClO ₄ + 0.5 M CH ₃ CH ₂ OH at room temperature with a scan rate of 50 mV/s. | 39 |
| Figure 20. Anodic part of the cyclic voltammogram of catalysts Ia, IIa, IIIa and Pt/ C in 0.1 M HClO ₄ + 0.5 M CH ₃ OH at room temperature. Scan rate is 50 mV/s. | 40 |
| Figure 21. Anodic part of the cyclic voltammogram of catalysts Ia, IIa, IIIa and Pt/ C in 0.1 M HClO ₄ + 0.5 M CH ₃ CH ₂ OH at room temperature. Scan rate is 50 mV/s. | 41 |
| Figure 22. Anodic part of the cyclic voltammogram of catalysts Ib, IIb, IIIb and Pt/ C in 0.1 M HClO ₄ + 0.5 M CH ₃ OH at room temperature. Scan rate is 50 mV/s. | 41 |
| Figure 23. Anodic part of the cyclic voltammogram of catalysts Ib, IIb, IIIb and Pt/ C in 0.1 M HClO ₄ + 0.5 M CH ₃ CH ₂ OH at room temperature. Scan rate is 50 mV/s. | 42 |
| Figure 24. Chronoamperometric curves of methanol oxidation on catalyst Ia (a), IIa (b), IIIa (c) and Pt/C(a) (d) at 0.5 V (vs. SCE) in 0.1 M HClO ₄ + 0.5 M CH ₃ OH. | 44 |
| Figure 25. Chronoamperometric curves of methanol oxidation on catalyst Ib (e), IIb (f), IIIb (g) and Pt/C(b) (h) at 0.5 V (vs. SCE) in 0.1 M HClO ₄ + 0.5 M CH ₃ OH. | 44 |

CHAPTER 1

INTRODUCTION

1.1. FUEL CELLS AND THEIR SIGNIFICANCE FOR THE ECONOMY

A *fuel cell* is more precisely a device than one of a variety of electrochemical power sources (EPSs), designed to convert chemical energy of the chemical reaction directly to electrical energy. The name 'fuel cell' is originated from the possible reactants or fuels that are natural types of fuels, needed for the current-producing reaction or products of fuel processing.

Fuel cells vary from other EPSs in a way that a fuel cell performs without periodic replacement or recharging for a rather extended time in contrast to batteries and accumulators when these two galvanic cells are taken into consideration.

Fuel cells are widely used throughout the economy and have a great importance. In the utilization of natural fuels for large-scale power generation (in megawatt power plants), fuel cells provide extremely higher efficiency and adequate abatement in the exhaust of combustion products and contaminants into the atmosphere from conventional thermal power plants. Moreover, fuel cells offer enhanced operation of power grids for temporary power storage by the help of load leveling with large-scale plants. The use of fuel cells also suggest widely developed grid power plants, which are decentralized, silent and local, as a power supply or as a combined power and for remote locations, buildings or installations, which are not connected to a grid, as a heat supply and lastly for individual installations as an emergency power. A significant enhancement in the ecological situation in densely populated regions is

lead by traction power plants for large-scale introduction of electric cars with a capacity of tens of kilowatts. In addition to these, providing crews of spacecrafts, submarines etc. drinking water besides supplying these structures with power installations. Last but not least, fuel cells offer small power units (with a capacity of tens or watts or milliwatts) for portable and transportable devices used in daily life or industrial applications such as mobile communication devices and signaling and controlling equipment respectively.

For all these reasons, the attention for the development of fuel cells has increased starting from the end of the nineteenth century. During the middle of twentieth century, declining world sources of oils and encountered ecological problems led the interest for fuel cells to become more global and general. From the 1950s and afterwards space explorations played a crucial role in terms of being a singular stimulus. Another stimulus arose towards the end of twentieth century with the advent of portable and other small devices which required an autonomous power supply over extended periods of use for civil and military purposes.

The great interests for the fuel cells are due to an important contribution of them towards solving economic and ecological problems that are encountered by the human kind. Doubtlessly, fuel cells are going to keep on contributing in the future. As a result of this interest for fuel cells, in many countries there are research and development centers such as science centers, university laboratories, national laboratories and industrial institutions in order to contribute development of fuel cells and make their use applicable.¹

1.2. THE LONG HISTORY OF FUEL CELLS

In 1791, the Italian physiologist Luigi Galvani conducted remarkable experiments demonstrating that muscle contraction will occur, similar to that produced by discharge of a Leyden jar, by the touch of two metals to the exposed frog nerve. This phenomenon partially interpreted by the Italian physicist Alessandro Volta in 1792.

Volta demonstrated that the contacts between these two metals and between these two and the muscle tissue generate this galvanic effect. On the basis of this phenomenon, in March 1800, Volta reported a device design based on the metal contact which could result in “inexhaustible electric charge”.

This device, now known as Volta pile, was the first example of an electrochemical device, in other words, an electrochemical power source that is battery. The volta pile has a great importance for the developments of science fields of electricity and electrochemistry since a new concept thus far not known which is “a continuous electric current” could now be realized. The properties and effects of electric current including many electrochemical processes were found within a short time. Electrolysis of water with production of hydrogen and oxygen were performed in May 1801, by William Nicholson and Sir Anthony Carlisle.

In the 1830s, not only a trained lawyer and judge but also an amateur natural scientist British Sir William Robert Grove (1811-1896) carried out a series of experiments about water electrolysis. The design of his device is given in Figure 1 and this device was prepared by using two platinum electrodes which were dipped into acidified water (by sulfuric acid). He made an assumption stating that if water can be electrolyzed due to a current pass then the opposite reaction may also take place. He observed the polarization of electrodes on which hydrogen and oxygen had been evolved as gases after disconnecting the current, in other words, between the electrodes potential difference was maintained. As a next step, when these two electrodes were connected to an external circuit, flow of current in the circuit was realized and this invention was named as a *gas voltaic battery* by Grove. February 1839, on which Grove’s results appeared in the *Philosophical Magazine* thought to be the creation date of the first fuel cell prototype.¹

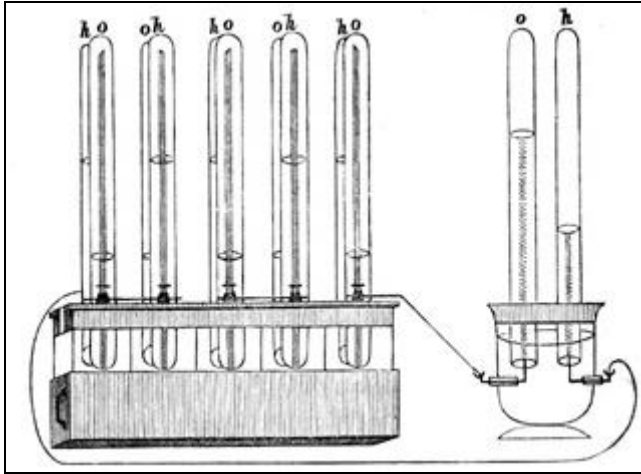


Figure 1. Grove's gas battery (1839).²

Lord Rayleigh developed a new form of gas battery (1882) and his main goal was to increase the surface of action between the solid electrode, the liquid and the gas in order to enhance the efficiency of the used platinum electrodes. Rayleigh used not only hydrogen as a fuel but also utilized coal and the current produced by this gas battery was considerable although it is inferior.

Fifty years later in 1889, another approach to form a new gas battery was presented by Ludwig Mond and Carl Langer. This new form of gas battery was the prototype for practical fuel cell and remarkably this new form is more than an enhancement. Electrode flooding problem which arose from a liquid electrolyte was overcome by the use of sulfuric acid for matrix formation, namely diaphragm, acting as a porous nonconducting solid. In order to maintain fuel cell reaction Mond and Langer focused on developing practical hardware. They understood that the internal resistance would result in the voltage decrease across the two electrodes.³

In 1894, when only 10 % chemical energy conversion of coal to mechanical energy was performed by steam engine, Oswald thought of electrochemistry as a solution to this low yield energy conversion. He proposed that using electrochemistry in order to

convert the chemical energy of coal without heat would provide the entire energy content of coal to be maintained since the steam engine process required heat to burn the coal and this heat was lost without having been conserved. However, Oswald's approach remained in theoretical since it was uncertain how to create the galvanic cell for this purpose.

In 1896, construction of fuel cells producing electricity from coal was performed by William Jacques. However, in 1904 Haber and Bruner were the first to conclude the electrochemical reaction between the coal and electrolyte then with electrode which was an indirect oxidation of coal. Lately, they focused their research on direct coal fuel cells. Baur and Ehrenberg conducted several experiments (in 1912) to find a suitable electrolyte among hydroxide, carbonate, silicate and borate after selecting an appropriate cathode, namely molten silver.

Just after the investigation of Baur and Ehrenberg, Baur and Brunner's research centered on the enhancement of the fuel cell starting from 1935 to 1937. They asserted that supplement of CO_2 to cathode resulted in a better performance. They determined that use of solid electrolyte rather than the molten one was more convenient since use of molten electrodes ended up with the flooding of electrodes. As a result, their interest was focused on ceramic materials.

In 1930s the Armenian scientist Oganess Davtyan developed an electrolyte in order to obtain a highly conducting and stable electrolyte that consists of several compounds. He designed a cell and conducted several experiment for both high temperature and low temperature fuel cells. He presented a book containing all his studies and this book was the first book in the world about fuel cells that was published in 1947.

Francis Thomas Bacon in 1932 started his studies out modifying the battery designed by Mond and Langer. Bacon's modification was based on selection of KOH (alkaline) electrolyte instead of using acid solutions (causing corrosion). Gas diffusion type porous electrodes were preferred in order to keep gases away breaking

through these electrodes and the electrolyte side was coated with gas permeable barrier layer having fine pores allowing gas diffusion. He took out patent of his design as *Bacon cell* in 1959. Bacon's cell inspired many other scientists as well and Grubb and Niedrach's (1960) and Grubb and Michalske's (1964) works based on this inspiration indicated the electrochemical oxidation of hydrocarbons was possible by using platinum electrodes below 150°C for the first time.

Aroused considerable interest for fuel cells can be attributed to the oil crisis burst out in the late 1960s and became more severely felt in 1973. At this point, natural fuel resources were to gain currency as an alternative energy source. Another stimulus was in charge to trigger the development of use of fuel cells since United States and Union of Soviet Socialist Republics were space racing starting from 1960s and Cold War years. In the early 1960s, Pratt and Whitney's company (the aircraft and engine manufacturer) licensed Bacon's work (development of the Alkaline Fuel Cell (AFC) for the Apollo spacecraft fuel cells. Alkali cells have then been in use for most subsequent manned U.S. space missions.¹

In the early 1960s, in the United States (US), National Aeronautics and Space Administration (NASA) were in search to power a series of manned space flights. Use of batteries, solar energy and at a time nuclear energy had many drawbacks for this kind of flights. Thus, fuel cells appeared to be an alternative energy and NASA launched sponsorships to develop this new technology in order to make its use possible and applicable for the space flights. These efforts played an important role in the development of the first Proton Exchange Membrane Fuel Cell (PEMFC).

Towards the end of the 1950s, modification of the fuel cell design with the use of solid ion- exchange membrane as an electrolyte was performed by a scientist namely, Willard Thomas Grubb who was a head of a group at General Electric (GE). Due to this development another scientist working at GE, Leonard Niedrach, found a way to deposit platinum on this membrane. The final devise designed started to be known as "Grubb-Niedrach fuel cell". Cooperation of NASA and GE for further development

of this inventory yielded results and the further developed fuel cell used for electric power generation in Gemini space project.

During the 1970s, fuel cell technology was enhanced for systems on Earth. The oil embargos of 1973 and 1979 acted as a stimulus for the research effort of the fuel cell since the desire for being independent of petroleum imports led U.S. Government to make investments to this new technology. For the commercialization of the fuel cells many companies and government organizations dedicated great effort after then. During 1970s and 1980s the focus of the researches was centered on the development of needed materials, optimization for the fuel sources and reduction of the high cost. During the 1980s, fuel cell technology started to get employed by automobile manufacturers. Ballard, the Canadian company, developed of the first marketable fuel cell-powered vehicle in 1993.

1.3. TYPES OF FUEL CELLS

Fuel cells can be divided into five major types depending on the type of the electrolyte used. These types are phosphoric acid fuel cell (PAFC), polymer electrolyte membrane fuel cell (PEMFC), alkaline fuel cell (AFC), molten carbonate fuel cell (MCFC) and solid-oxide fuel cell (SOFC). The operation of all these fuel cells depends on the same basic concept in which at anode oxidation of fuel into electrons and protons take place while at cathode the reduction of oxygen to oxidized species occurs. Transportation of either protons or oxide species through the ion-conducting (but electronically insulating) electrolyte to generate water and electric power by combining with oxide or protons depends on the type of the electrolyte used.^{3,4,5}

Table 1. Types of fuel cells and their major characteristics with their fields of application areas.⁵

| Fuel Cell Type | Common Electrolyte | Operating Temperature | Electrical Efficiency | Combined Heat and Power (CHP) Efficiency | Applications | Advantages |
|--|---|-------------------------------|--|--|---|---|
| Polymer Electrolyte Membrane (PEM)* | Solid organic polymer poly-perfluorosulfonic acid | 50 - 100°C 122 - 212°F | 53-58% (transportation) 25-35% (stationary) | 70-90% (low-grade waste heat) | -Backup power -Portable power -Small distributed generation -Transportation -Specialty vehicles | -Solid electrolyte reduces corrosion & electrolyte management problems - Low temperature - Quick start-up |
| Alkaline (AFC) | Aqueous solution of potassium hydroxide soaked in a matrix | 90 - 100°C 194 - 212°F | 60% | >80% (low-grade waste heat) | - Military - Space | - Cathode reaction faster in alkaline electrolyte, leads to higher performance -Can use a variety of catalysts |
| Phosphoric Acid (PAFC) | Liquid phosphoric acid soaked in a matrix | 150 - 200°C 302 - 392°F | >40% | >85% | -Distributed generation | - Higher overall efficiency with CHP - Increased tolerance to impurities in hydrogen |
| Molten Carbonate (MCFC) | Liquid solution of lithium, sodium, and/or potassium carbonates, soaked in a matrix | 600 - 700°C 1112 - 1292°F | 45-47% | >80% | - Electric utility - Large distributed generation | - High efficiency - Fuel flexibility - Can use a variety of catalysts - Suitable for CHP |
| Solid Oxide (SOFC) | Ytria stabilized zirconia | 600 - 1000°C 1202 - 1832°F | 35-43% | <90% | - Auxiliary power - Electric utility - Large distributed generation | - High efficiency - Fuel flexibility - Can use a variety of catalysts - Solid electrolyte reduces electrolyte management problems - Suitable for CHP - Hybrid/GT cycle |

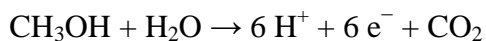
* Direct Methanol and Ethanol Fuel Cells are a subset of PEM typically used for small portable power applications with a size range of about subwatt to 100 W and operating at 60-90°C.

1.4. THE DIRECT METHANOL FUEL CELLS

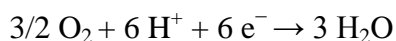
In the last decade, considerable attention was directed to the direct electrochemical oxidation of alcohols and hydrocarbons. Organic liquid fuels have great importance due to their high energy density and among these liquid fuels; methanol is the promising candidate in terms of reactivity at low temperatures, storage, readily availability, high energy density, handling and absence of by products except CO₂. Moreover, there appear specific advantages of direct methanol fuel cells (DMFCs) over hydrogen based fuel cells such as simple handling, easy storage, and high energy density (stored) and those make DMFCs a suitable new candidate for the fuel cell technology⁶. Therefore, these advantages of methanol makes it prior for its application through mobile power plants and to a great extent small low power fuel cells as a power supply to electronic devices such as personal computers and mobile phones. In addition to these, methanol has a high electrochemical activity and has a satisfactory specific energy content those even make its use possible for large power plants in electric vehicles.¹

Protonic membranes used DMFCs are directly supplied by methanol and water at the anode on which oxidation of methanol to carbon dioxide takes place while at the cathode reduction of oxygen to water occurs as illustrated in Figure 2. The reactions taking place both at the anode and cathode and the overall reaction are⁶:

Reaction takes place at the anode compartment:



Reaction takes place at the cathode compartment:



Overall Reaction:

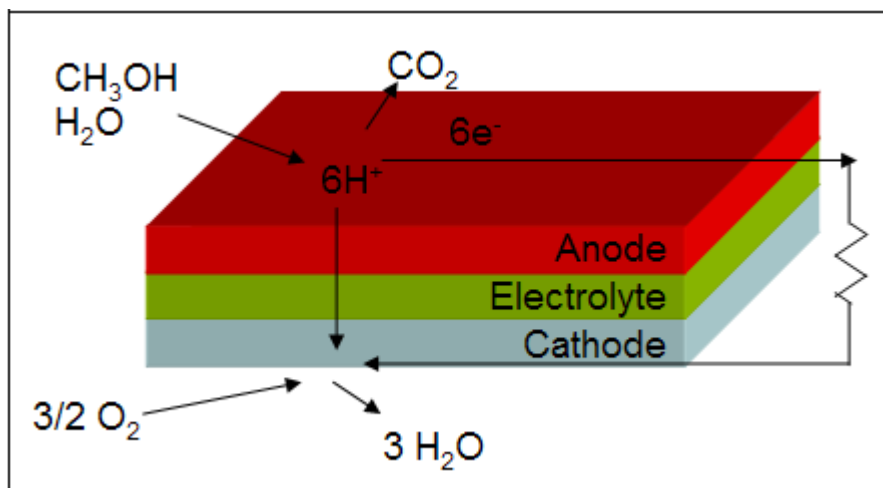
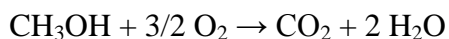


Figure 2 Schematic representation of a DMFC.⁷

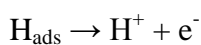
Although the major reaction product is carbon dioxide, there are some other side-products in small amounts are observed in certain cases. Methanol oxidation is not a single step reaction that consists of sequential stages. First, dehydrogenation of methanol molecules to chemisorbed species, COH_{ads} , takes place:



Then, oxidation of these adsorbed species occurs by the adsorbed oxygen-containing species (OH_{ads} on the neighboring sites of platinum surface):



The steps at which the current is produced arise from the ionization of adsorbed hydrogen atoms and anodic formation of water sourced OH_{ads} species:



At some points the formation of OH_{ads} species is not possible therefore, COH_{ads} species age in time to turn into CO_{ads} species which result in poisoning of the catalyst since oxidation of CO_{ads} species are not easy and this causes inhibition of methanol oxidation.

Although the great advantages of DMFCs, there are still some problems to be solved to make its application possible in a wide range. The slow reaction rate of DMFCs and inadequate lifetime researches dedicated to DMFCs are the present problems. Moreover, as mentioned earlier, aging of the methanol is one of the drawbacks leading to a drastic slowdown of the oxidation reaction. High cost of the used catalyst, platinum, should be lowered by the use of other catalysts (Ru, Mo, Ni, Pd) or use of platinum with second or third metal to form an alloy which also provides low oxidation potential and alternative sites for the oxidation reactions. Methanol's being toxic is also one of the disadvantages of DMFCs; necessary precautions should be taken in order to prevent any leakage from the prepared cells.¹

1.5. THE DIRECT ETHANOL FUEL CELLS

Ethanol offers an attractive alternative candidate as a fuel for direct ethanol fuel cells (DEFCs) due to numerous advantages it has. It is less toxic compared to methanol and has high energy density. Moreover, ethanol can easily be produced by the fermentation of various agricultural biomasses. At this point, it is to be stated that during hot combustion reactions (uses of fuels in heat engines) and also cold combustion reactions (electrochemical uses of fuels) evolution of CO_2 is inevitable and this evolution causes a well known effect namely, global warming. As

mentioned, since the production of ethanol is provided by fermentation of biomasses and the photosynthesis reaction of these biomasses require the use of CO_2 and solar energy.

It is true to state that ethanol is unique among the fuels due to its being renewable. Because of this important characteristic of ethanol, production of it from biomass study has begun in Brazil in order to replace ethanol with gasoline in large part of the automotive transport sector just after the needed infrastructure studies and transformation of the transport vehicles to make their use convenient with ethanol were completed. In addition to the study done in Brazil, also in the European Union, ethanol has been addressed as an attractive alternative fuel.^{1,8} However, there are still some problems to be solved in DEFCs briefly, requirement of high working temperature in DEFCs and high cost of the catalyst used.

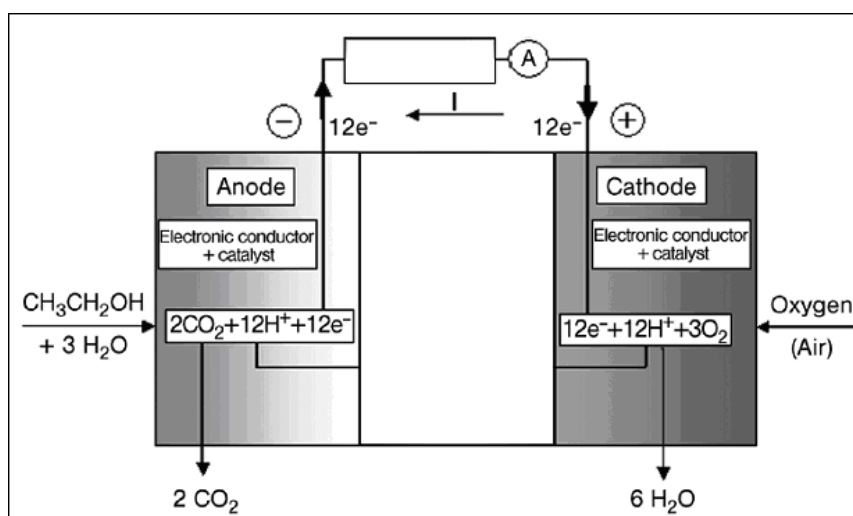
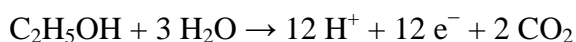


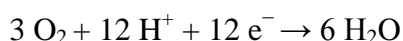
Figure 3. Schematic diagram of a DEFC.⁹

The reactions taking place at the anode compartment and cathode compartment are shown in the Figure 3 and the reactions are as follows⁹:

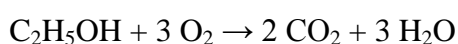
Reaction takes place at the anode compartment:



Reaction takes place at the cathode compartment:



Overall Reaction:



The complete electro-oxidation of ethanol to CO_2 includes 12 electrons per molecule and many adsorbed intermediates. In addition to this, ethanol electro oxidation occurs through different pathways on different catalytic surfaces or in different media. Therefore, proposal of exact mechanism of ethanol electrooxidation is quite difficult.¹⁰

The main problem encountered for the direct ethanol fuel cells is the required high working temperature due to the low reactivity of ethanol. Furthermore, as mentioned above difficulties are present in term of complete electro oxidation of ethanol to CO_2 which arise from the challenge encountered for the breaking of C-C bond that is not easy to perform especially in low temperatures. The other problems faced with are similar to those of DMFCs as described in part 1.4, briefly high cost of used catalysts, aging of the catalyst used.

In order to overcome the major problems encountered for both DMFCs and DEFCs, the fundamental efforts and researches have been addressed to the development of

anode catalyst due to the poor electrochemical activity of the starting reagent (alcohol) in acidic solution at low potentials. Mainly, Pt based catalysts have been employed for the electro oxidation of methanol and ethanol. However, there has been a growing interest for the search of more active materials recently. A prepared new catalyst should allow alcohol oxidation reaction to operate at low temperature and at low potentials.¹¹

Since the platinum comes into view as the most active catalyst for the alcohol oxidation reactions, addition of second metal to Pt in order to form an alloy has been under investigation. Researches were mainly focused on a development of a binary Pt catalyst by use of Pd, Ru, Rh, Re, or Sn as second metal.^{12,13,14,15} Among these metals, use of Pd as a second metal comes into prominence due to its high abundance on earth and its being a good electrocatalysts for the oxidation reactions of organic fuels. It should also be noted that, by the use of palladium, surface concentration of the adsorbed intermediate species can be lowered by means of releasing the occluded hydrogen that is present in palladium.¹⁴

1.6. THE OBJECTIVE OF STUDY

In this thesis, two groups of carbon supported nano-sized Pt-Pd catalysts, group “a” & “b”, have been synthesized for the oxidation reactions of methanol and ethanol in acidic medium. Besides, effect of Pd as a second metal and the effect of the used surfactants on the size of the metal nanoparticles and the catalytic activity were investigated. For group “a” and “b” catalysts, 1-hexanethiol and 1,1 dimethyl hexanethiol was used for the first time as stabilizing agents for Pt-Pd catalysts, respectively. Cyclic voltammetry (CV), chronoamperometry (CA), X-ray diffraction (XRD), transmission electron microscopy (TEM), X-ray photoelectron spectroscopy (XPS) were employed for the characterization of the prepared catalysts. The effect of the type of the used surfactant on the size and catalytic activity has been determined. Furthermore, electrochemical methods were used for the determination of the catalytic activities of the synthesized Pt-Pd catalysts.

CHAPTER 2

EXPERIMENTAL

2.1. SYNTHESIS OF CATALYSTS

2.1.1. SYNTHESIS OF CATALYST Ia

Dissolving 0.24 mmol (0.0808 g) of PtCl₄ (99 %, Alfa) and 0.050 mmol (0.0090 g) PdCl₂ (59 % Sigma) in 25 ml of anhydrous tetrahydrofuran (THF, 99.5 %, Merck) for an hour under high-purity argon atmosphere was the first step. Second, addition of 0.27 mmol (39 μL) of 1-hexanethiol (C₆H₁₃SH, 95 %, Merck) as a surfactant to this solution was pursued and the mixture was stirred vigorously for 2.5 hours. Finally, reduction of thiol stabilized bimetallic complex was done by the drop wise addition of lithium triethylborohydride (superhydride, 1.0 M dissolved in THF, Aldrich). Color change from yellowish to the dark black was an indication of formation of Pt-Pd nanoparticles therefore addition of superhydride was maintained till this color change was observed.¹⁶

Washing process with dry ethanol (99.9 %, Merck) in ultrasonic bath was applied to the resulting solution in order to remove excess thiols.¹⁷ To remove the organic residues over precipitate centrifugation was performed. This process was repeated until a clear filtrate solution was observed. Consequently, the solid precipitate was dried under vacuum at room temperature.

2.1.2. SYNTHESIS OF CATALYSTS IIa, IIIa, Ib, IIb, IIIb

An appropriate amount of PtCl₄ (99 %, Alfa) and PdCl₂ (59 % Sigma) (shown in Table 2) were used in order to prepare the catalysts IIa, IIIa, Ib, IIb, IIIb by using the same procedure as described in section 2.1.1.

2.1.3. SYNTHESIS OF Pt/C (a & b)

In the early and published work performed in our group, Pt/C (a) and Pt/C (b) were prepared by superhydride reduction method using 1-hexanethiol, 1,1 dimethyl hexanethiol as surfactants, respectively.¹⁸

Table 2. Platinum complexes and surfactants used for all prepared catalysts.

| Catalysts | Surfactants | Pt / Pd Nominal Ratios | Atomic % Ratios of Pt/Pd (ICP) |
|----------------------|--------------------------|-----------------------------------|---|
| Pt/C (a) | 1-Hexanethiol | | |
| Catalyst Ia | 1-Hexanethiol | 90% / 10% | 87.4% / 12.6% |
| Catalyst IIa | 1-Hexanethiol | 80% / 20% | 76.8% / 23.2% |
| Catalyst IIIa | 1-Hexanethiol | 70% / 30% | 65.1%/34.9% |
| Pt/C (b) | 1,1 dimethyl hexanethiol | | |
| Catalyst Ib | 1,1 dimethyl hexanethiol | 90% / 10% | 88.2%/ 11.8% |
| Catalyst IIb | 1,1 dimethyl hexanethiol | 80% / 20% | 81.3% / 18.7% |
| Catalyst IIIb | 1,1 dimethyl hexanethiol | 70% / 30% | 72.1% / 27.9% |

2.2. ELECTRODE PREPARATION

By mixing 36.78 mg of prepared carbon supported powder catalyst, 0.5 mL of Nafion (Aldrich, 5 wt %), 0.15 mL of N,N-dimethyl formamide (Merck, 99.5 %) and 2.5 mL of distilled water, a mixture was obtained. This solution was sonicated in ultrasonic bath till an almost slurry mixture was observed due to the dispersion of the solid in this solution. 50 μ L of the slurry solution was employed on 0.7 cm (diameter) of glassy carbon for the purpose of using it as a working electrode. Then drying process was applied by increasing the temperature from 40°C (20 minutes) to 65°C (20 minutes) and finally further heated to 100°C (1 hour) to provide good ‘adhesion’ of the catalyst to the surface of the glassy carbon electrode.

2.3. PLATINUM & PALLADIUM CONTENT DETERMINATION

The amount of platinum and palladium in each catalyst was determined by Leeman Lab inductively coupled plasma spectroscopy (ICP) (Central Lab., METU).

2.4. CHARACTERIZATION TECHNIQUES

2.4.1. CYCLIC VOLTAMMETRY (CV)

In order to obtain both qualitative and quantitative information about electrochemical reactions, cyclic voltammetry (CV) is the one most widely applied among electrochemical techniques. *Redox potentials* of the electro active species are easily determined by CV. Characterization of the peak or couple can be studied not only from the potentials of peaks on cyclic voltammograms but also from the changes evoked by the scan rate variation.

Most probably, CV is the first technique to employ in an electrochemical study. CV measurements are executed by implementing a repetitive triangular potential

excitation signal which results in a sweep back and forth between two switching potentials on working electrode's potential (Figure 4).^{19,20}

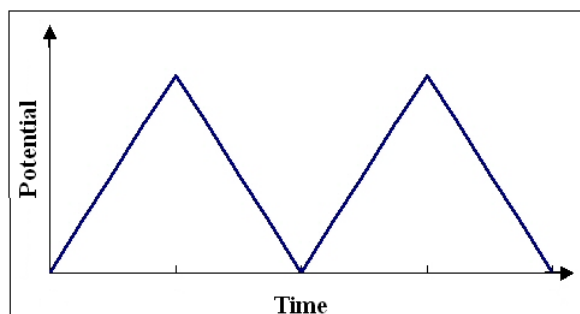


Figure 4. Typical excitation signal for cyclic voltammetry.²¹

The main working principle of this technique depends on the variation of the applied potential exerted on a working electrode in both forward and backward scans. In typical cyclic voltammetry, electron transfer is driven by the surface's adequate positivity or negativity in voltage which caused by the electrolyzation (oxidation or reduction) of the solution component by the touch of the solution with the electrode surface. In simple cases, a particular voltage is exerted on the surface at the beginning with respect to a reference such as calomel or Ag/AgCl and the electrode voltage is varied linearly in both forward and backward scans. Due to this variation in voltage, surface becomes adequately positive or negative through which electron transfer takes place between the chemical species and the surface. This gives rise to a measurable current in the circuit. As a result of the reversed voltage cycle, electron transfer is also reversed and resulting in an inverse current peak. Depending on the analysis, one full cycle, a partial cycle, or a series of cycles can be executed and the current at the working electrode is measured through the potential scan so as to acquire a cyclic voltammogram.^{20,22} A typical cyclic voltammogram showing the reduction and oxidation current peaks is given in Figure 5.

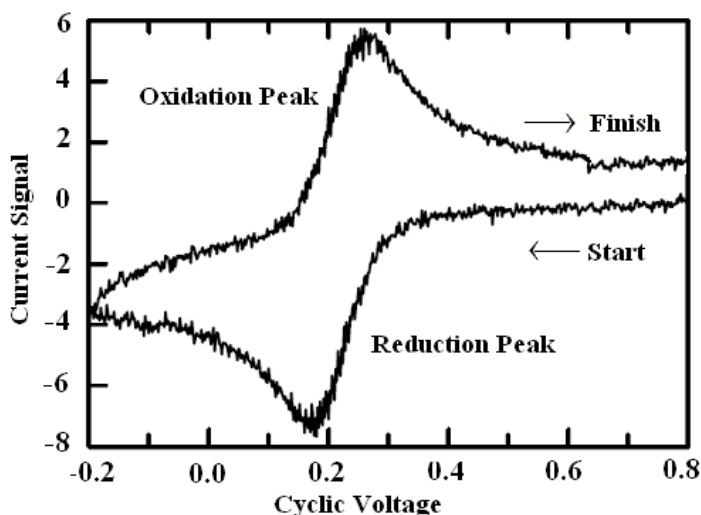


Figure 5. A typical cyclic voltammogram displaying reduction and oxidation current peaks.²³

2.4.1.1. ELECTROCHEMICAL CELL

Execution of cyclic voltammetry measurements were held by the use of a microcomputer-controlled potentiostat/galvanostat, Solartron 1285, at room temperature (Department of Chemistry, METU). The saturated calomel electrode (SCE), glassy carbon and prepared catalysts were used as a reference, counter and working electrodes, respectively. 0.1 M HClO₄ (60 %, Merck) + 0.5 M CH₃OH (99.9 %) or 0.1 M HClO₄ (60 %, Merck) + 0.5 M CH₃CH₂OH (99.2 %) solutions were utilized as an electrolyte. In order to remove the oxygen in the electrolyte and in the cell, pure argon was passed through the electrolyte for fifteen minutes before the measurements were taken.

2.4.2. CHRONOAMPEROMETRY (CA)

Stability of the compound's initial redox state can be tested in a potential range by monitoring the switching on current with time that is chronoamperometry (CA). This basic technique provides important information by distinguishing the capacitive

current from higher Faradaic currents that are taking place during oxidation and reduction processes in the potential range given. CA studies are executed by employing an excitation signal which is a square-wave voltage signal which steps the potential of the working electrode from a value where no faradaic current occurs to a potential at which the surface concentration of the species is effectively zero. The current decay is observed when the electrodes are charged to the applied potential. ^{20,22}

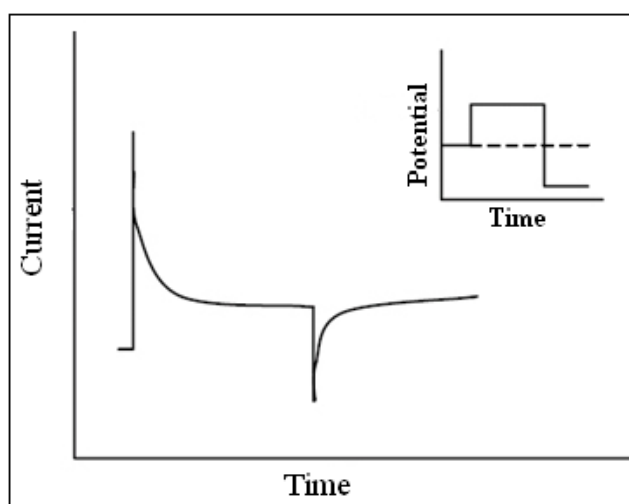


Figure 6. A typical chronoamperogram. Inset is the excitation waveform.²²

In this study, as electrochemical techniques, cyclic voltammetry (CV) and chronoamperometry (CA) were utilized by using a microcomputer-controlled potentiostat/galvanostat, Solartron 1285, at room temperature. The reference, counter and working electrodes were assigned as the saturated calomel electrode (SCE), glassy carbon and prepared catalysts respectively (Department of Chemistry, METU).

2.4.3. X-RAY DIFFRACTION

X-ray diffraction is a very powerful, analytical and nondestructive method used for the examination of fingerprint characterization and structure determination. X-ray diffraction is used for the determination of the actual arrangement of atoms within a crystalline specimen. Among the theories and equations about the main concept of this technique, Bragg law is the easiest one for demonstrating the diffraction of X-rays by a crystal. The diffraction peak appears under certain conditions satisfying the Bragg condition:

$$2d\sin\theta = n\lambda$$

where; λ , θ , n and d are wavelength of the x-ray, the Bragg angle at where diffraction peak is observed, an integer representing the order of the diffraction peak and the distance between atomic planes, respectively^{24,25}, Figure 7.

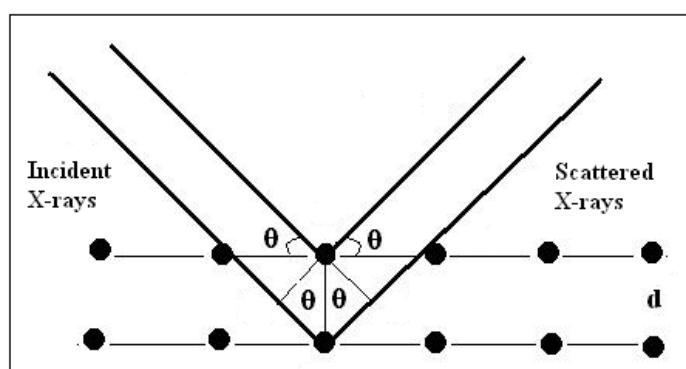


Figure 7. The incident and scattered X-rays.²⁶

Two major X-ray techniques is available for X-ray diffraction namely, single crystal and powder methods. Single crystal X-ray diffraction is a technique used to

determine the structure of crystalline materials including inorganic compounds and complex macromolecules like proteins or polymers. Single crystal is required to discover the nature of the crystal structure.

Single crystal X-ray crystallography plays a crucial role in terms of the determination of molecular conformations of biological species; however, acquisition of a single crystal is so tough. In addition to this, this method offers advantages that diffraction peaks from only the selected crystal plane are observed which makes the characterization easier.

On the other hand, powder X-ray diffraction is applied for the characterization of crystallographic structure, grain size, and preferred orientation in polycrystalline or powder solid samples.²⁴ Unknown crystalline materials can be analyzed by the help of this method in terms of making comparison of the diffraction data of the compounds with the database (International Centre for Diffraction Data (ICDD)) of the known materials.

As pointed out earlier in this section, X-ray diffraction is a powerful tool to employ not only for the fingerprint characterization but also for the structure and size determination. In this study, the average particle sizes of the prepared Pt-Pd catalysts were calculated from the X-ray diffraction pattern by using Scherrer formula:

$$d (\text{\AA}) = \frac{k\lambda}{\beta \cos\theta}$$

where k is a coefficient (0.9), λ is the wavelength of X-ray (1.54056 Å), β is the full width half-maximum of respective diffraction peak (rad) and θ is the angle at the position of peak maximum (rad). Rigaku diffractometer with Ultima + theta-theta high resolution goniometer, the X-ray generator (Cu K α radiation, $\lambda = 1.54056\text{\AA}$) with an operation conditions at 40 kV and 40 mA were employed for the X-ray diffraction analysis (Central Lab., METU).

2.4.4. TRANSMISSION ELECTRON MICROSCOPY (TEM) AND ENERGY DISPERSIVE X-RAY SPECTROSCOPY (EDS)

Transmission Electron Microscopy (TEM) is a well known and widely used technique employed in order to obtain an image of solid materials at atomic resolution. Acquisition of structural information can be performed not only by imaging but also by electron diffraction. Elemental and chemical analysis down to this sub-nanometer scale is possible by the implementation of additional detectors.

The design of the transmission electron microscope is an optically analogous to the design of conventional light microscope. In TEM, a beam of high energy electrons is applied instead of photons and electromagnetic lenses instead of glass lenses. A beam of electrons pass through an electron transparent sample and by the use of set of lenses image is magnified and projected on to a screen. The lateral resolution is achieved for a resolution of 0.2 nm by the use of much smaller wavelength of electrons.

Image contrast is acquired by the interaction between the electron beam and the sample and the areas having high density and having heavier elements seem darker in a TEM image owing to the scattering of the electrons in the sample. Scattering from crystal planes also creates diffraction contrast that is presumably dependent on the orientation of a crystalline area in the sample. As a result, each crystal possesses its own grey-level which helps one to differentiate not only materials but also individual crystals and crystal defects in a sample having randomly oriented crystals. Atomic arrangements in crystalline structures can be examined in a detailed way by TEM due to its high resolution.

The first step in phase identification is a chemical analysis that can be done in a TEM microscope by *X-rays energy dispersive spectrometry*, EDS. The interaction between the incident electron beam and the sample evoke the emission of X-rays. The energies of the X-rays are specific for the atoms present in the volume that is probed.

Energy dispersive X-ray analysis is the name given to the detection and characterization of the X-rays. The elemental composition can be acquired by the X-ray spectrum in the irradiated area.^{27,28}

JEOL 200 kV TEM instrument was used to acquire transmission electron microscopy (TEM) images. Sample preparation for TEM analysis involved dispersion of carbon supported catalyst in ethanol by the use of ultrasonic bath and then placement of a drop of (~0.5 mg/mL) this solution on a carbon covered 400-mesh copper grid and the solvent was evaporated before TEM analysis (Central Lab., METU).

2.4.5. X-RAY PHOTOELECTRONSPECTROSCOPY (XPS)

X-ray Photoelectron Spectroscopy (XPS) is a surface analytical technique which is used in order to excite emission of photons, electrons or ions by the bombardment of the sample with photons, electrons or ions.

In XPS, generation of photoelectric effect is created by the low-energy (~1.5 keV) X-ray irradiation of the sample. High-resolution electron spectrometer is benefited in order to obtain the energy spectrum of the emitted photoelectrons. Vacuum conditions are needed for the sample analysis therefore; vacuum chamber is used not only for making the transmission of the photoelectrons to the analyzer easier but also and more essentially for decreasing the re-contamination rate of a cleaned sample. Owing to the high surface sensitivity of XPS analysis, with a typical “sampling depth” of only a few nanometers, employment of a vacuum is pivotal.

When the photoemission process is taken into consideration, the total energy of the system can be described as the sum of the energy of the X-ray photon ($h\nu$) and the energy of the target atom in its initial state, (E_i), just before the emission process. After the emission process, the total energy of the system can be defined as the sum of the total energy of the system is the kinetic energy of the photoelectron (E_k) plus that of the ionized atom in its final state (E_f) as shown in Figure 8.

$$h\nu + E_i = E_k(e^-) + E_f$$

$$h\nu - E_k(e^-) = E_f - E_i = E_b$$

By subtracting the $E_k(e^-)$ from $h\nu$ in the equation, the binding energy, E_b , of the electron is found to be the difference between the final state and initial state energies of the target atom $E_f - E_i$.^{29,30}

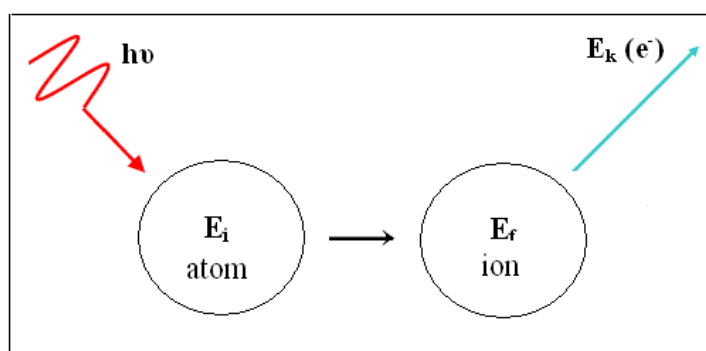


Figure 8. Illustration for the derivation of binding energy where E_k is the kinetic energy of the photoelectrons, E_i is the initial state and E_f is the final state.³⁰

In this study, Specs spectrometer was used for X-ray photoelectron spectroscopy (XPS) analysis and $K\alpha$ lines of Mg (1253.6 eV, 10 mA) were utilized as an X-ray source. All XPS peaks have been fitted by using Gaussian function and C 1s line at 284.6 eV was determined as a reference line (Central Lab., METU).

CHAPTER 3

RESULTS AND DISCUSSION

3.1. X-RAY DIFFRACTION (XRD) AND TRANSMISSION ELECTRON MICROSCOPY (TEM)

The crystal structure and average crystalline size of the metal particles of all prepared catalysts were explored by XRD. XRD data exhibited peaks that correspond to Pt (111), (200), (220), and (311) planes, which was an indication for the crystallization of Pt in face centered cubic (fcc) structure.³¹ Table 3 gives the peak positions of Pt (220), lattice parameters and atomic percent of platinum and palladium of all catalysts. As it is given in the table, all of the diffraction peaks were similar but a shift to higher 2θ values was observed for each catalyst compared to those of Pt¹⁸ which accounted for the formation of PtPd alloy in all catalysts. The lattice parameter ($a_{\text{Pt-Pd}}$) values of the catalysts were calculated from the following equation (equation 1), using Pt (220) diffraction peaks^{32,33} and also given in Table 3.

$$a = \frac{\lambda(\sqrt{h^2 + k^2 + l^2})}{2\sin\theta} \quad \text{for a cubic structure} \quad (1)$$

where a , λ , θ , (h k l) are the lattice parameter, the wavelength of X-ray used (1.54056 Å), the peak position in θ , the planes of atoms, respectively.

The calculation of lattice parameters indicated a decrease in the lattice parameters of Pt-Pd catalysts when compared to the Pt ones¹⁸, as illustrated in Figure 9, and this

also reflected the formation of an alloy, that is to say, incorporation of Pd into the Pt fcc structure. For this purpose, Vegard's law (equation 2) was applied in order to calculate the extent of alloy formation with respect to Pd amount used or incorporation ratio of Pd into the Pt fcc structure in all catalysts. The results are given in Table 3.1 and shown in Figure 9.

$$a_{(Pt-Pd)} = a_{(Pt)} - kx_{Pd} \quad (2)$$

where $a_{(Pt-Pd)}$, $a_{(Pt)}$, k and x_{Pd} are the lattice parameters of the Pt/Pd alloy, lattice parameter of Pt, lattice constant (0.124 Å) and atomic fraction of Pd, respectively.³⁴

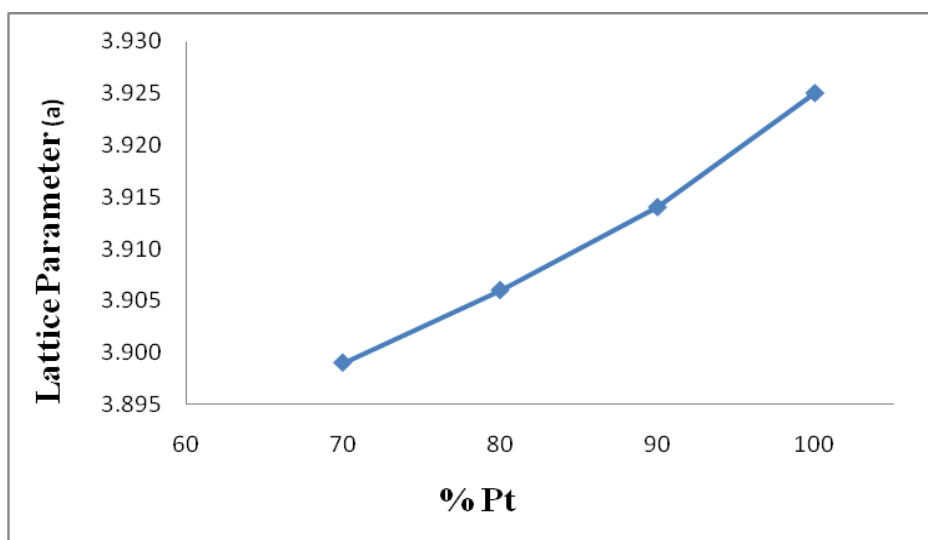


Figure 9. Dependence of fcc lattice constant (a in angstroms) on the Pt content of the Pt/C (b), catalyst Ib, catalyst IIb and catalyst IIIb.

The lattice parameters, $a = 0.392$ nm and $a = 0.389$ nm belong to Pt and Pd, respectively and Pt and Pd both crystallize in fcc structure. Owing to the smaller lattice parameter of Pd than that of Pt, Pd insertion into Pt fcc causes a decrease in the lattice parameters of all prepared catalysts and that is, formation of Pt-Pd alloy. The percent incorporation of Pd into Pt fcc structure (with respect to the Pd amount

used) was calculated and summarized in Table 3. The calculations revealed that the highest percent of Pd incorporation into Pt fcc structure with respect to the Pd amount used was observed for catalysts Ia and Ib (~ 83.3 and 89.0 %) in which most of the palladium used was incorporated in Pt fcc. Moreover, it should also be stated that the percent incorporation of Pd into Pt fcc structure was observed to be higher for group “b” catalysts than that of group “a” catalysts.

Table 3. Peak positions, lattice parameter, atomic percent of platinum and palladium in all catalysts.

| samples | (<i>hkl</i>) (220) ^a | <i>d</i> ^b (nm) | <i>a</i> ^c in Å | atomic % of Pt ^d | atomic % of Pd ^d | <i>x</i> _{Pd} ^e | incorporated Pd % ^f |
|---------------|--------------------------------------|-------------------------------|-------------------------------|--------------------------------|--------------------------------|-------------------------------------|-----------------------------------|
| Pt/C (a) | 67.40 | 0.1388 | 3.927 ± 0.014 | | | | |
| catalyst Ia | 67.65 | 0.1384 | 3.914 ± 0.012 | 87.4 | 12.6 | 10.5 | 83.3 |
| catalyst IIa | 67.80 | 0.1381 | 3.906 ± 0.009 | 76.8 | 23.2 | 16.9 | 72.8 |
| catalyst IIIa | 68.00 | 0.1377 | 3.896 ± 0.007 | 65.1 | 34.9 | 25.0 | 71.6 |
| Pt/C (b) | 67.50 | 0.1387 | 3.925 ± 0.012 | | | | |
| catalyst Ib | 67.70 | 0.1383 | 3.912 ± 0.010 | 88.2 | 11.8 | 10.5 | 89.0 |
| catalyst IIb | 67.85 | 0.1381 | 3.906 ± 0.012 | 81.3 | 18.7 | 15.3 | 81.8 |
| catalyst IIIb | 67.95 | 0.1378 | 3.900 ± 0.011 | 72.1 | 27.9 | 20.1 | 72.0 |

a) The peak positions of (220) in 2θ,

b) Calculated from Pt (220) peak according to Bragg formula,

c) Lattice parameters,

d) Atomic percent of platinum and palladium calculated from Pt and Pd elemental analyses,

e) Atomic fraction of Pd calculated by using XRD data,

f) Percent palladium which incorporated into Pt-Pd alloy in all catalysts.

In order to calculate the average crystalline sizes of the metal particles in the catalysts from the full width half maximum of the Pt (220) reflection peaks in XRD³⁵, Debye-Scherrer equation (equation 3) was used and the average crystalline sizes and were found to be as 3.00 ± 0.05 , 3.20 ± 0.07 and 3.50 ± 0.09 nm for catalyst Ia, IIa and IIIa, respectively; 3.20 ± 0.08 , 3.40 ± 0.11 and 3.70 ± 0.14 nm for catalyst Ib, IIb and IIIb, respectively. XRD diffraction pattern for Pt (220) plane is given in Figure 10.

$$d (\text{\AA}) = \frac{k\lambda}{\beta \cos\theta} \quad (3)$$

where k = a coefficient (0.9), λ = the wavelength of X-ray (1.54056 \AA), β = the full width half-maximum of respective diffraction peak (rad) and θ = the angle at the position of peak maximum (rad).

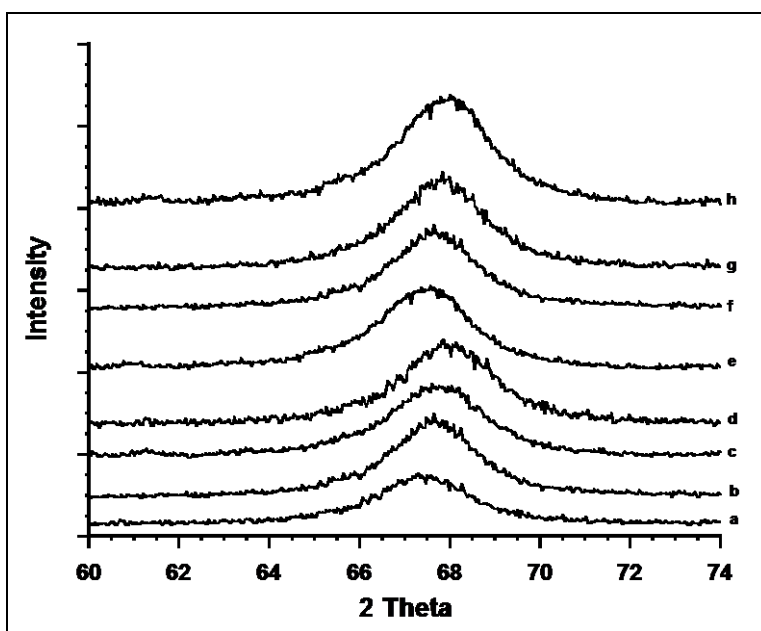


Figure 10. XRD diffraction pattern of Pt/C a (a), catalysts Ia (b), IIa (c), IIIa (d), Pt/C b (e), catalysts Ib (f), IIb (g) and IIIb (h).

Transmission electron microscopy was employed so as to observe the metal particle distributions and calculate average sizes of metal particles in the prepared catalysts. From TEM micrographs, it was found that all prepared Pt-Pd catalysts have uniform and narrow size distribution ranging from 3.0 to 3.7 nm (based on the observation of about 300 particles) on the carbon support and the particle size distributions are given in Figure 11.

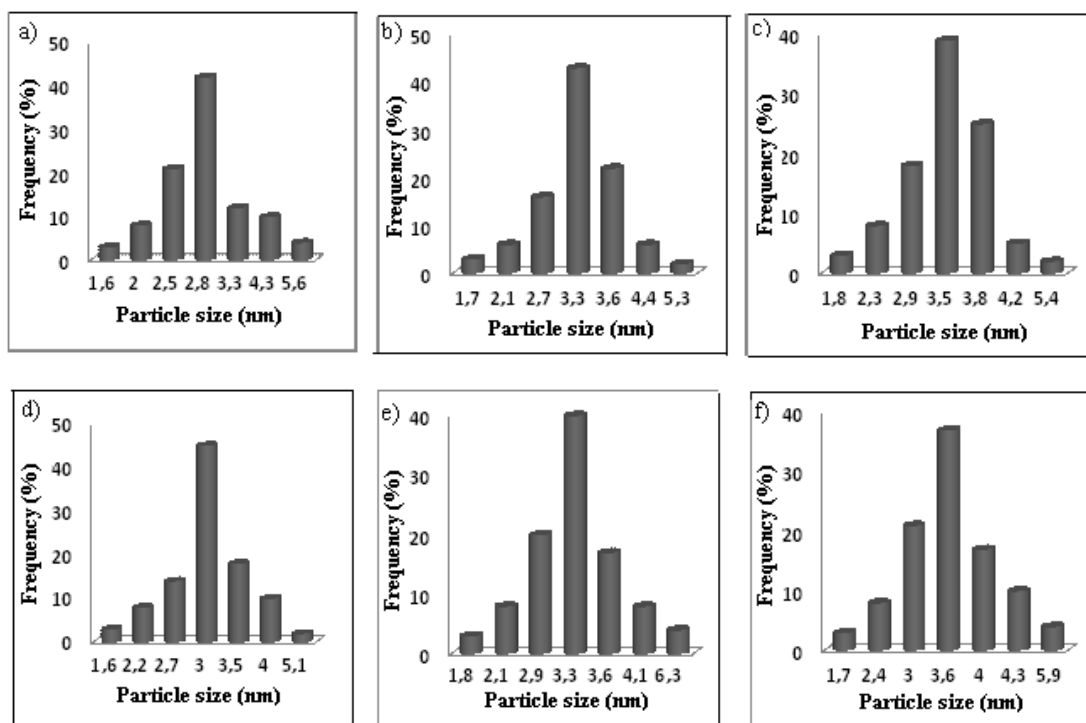


Figure 11. Size distribution of catalyst Ia (a), IIa (b), IIIa (c), Ib (d), IIb (e) and IIIb (f).

TEM results also revealed that the average crystalline sizes of metal particles obtained for group “b” catalysts were larger than that of group “a” catalysts. It can be explained by the surfactant structure effect that is, use of a branched surfactant may have a tendency to form a larger hole in the micelles which accounts for the larger

particle size formation. The case is reverse when the linear surfactant is utilized as a stabilizing agent and the both cases are illustrated in Figure 12.

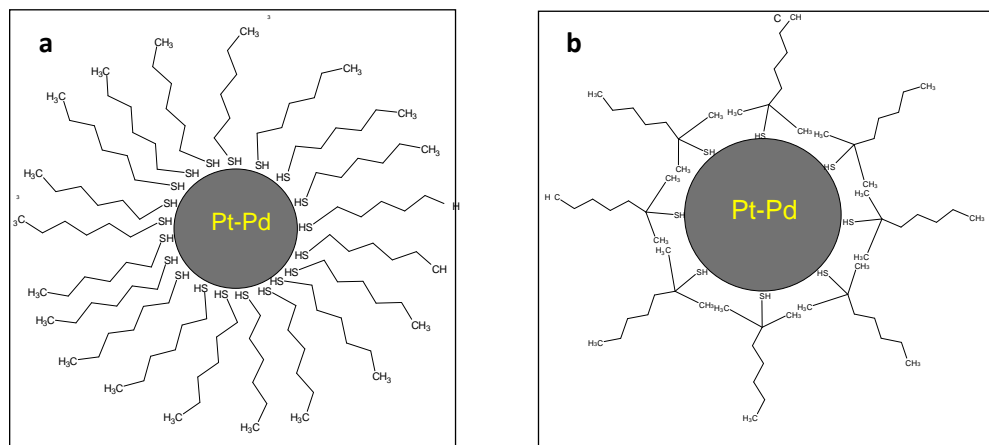


Figure 12. A schematic representation of the formation of the group ‘a’ and ‘b’ Pt-Pd nanoparticles.

The average particle size of metals, those calculated from XRD data and obtained from TEM analysis are not only in good agreement with each other’s but also with the ones obtained for Pt-Pd catalysts in the literature.^{10,15} TEM images also revealed the absence of agglomeration of the prepared Pt-Pd catalysts on carbon support. By the help of the high resolution TEM image, the well-defined crystalline nature of Pt-Pd catalysts can be obtained and the atomic lattice fringes were calculated and found to be as, for catalyst Ib, 0.220 and 0.194 nm which are very close to nominal Pt (1 1 1) and (2 0 0) spacing of 0.228 and 0.196 nm, respectively^{31,36} and shown in Figure 13 (a). In addition to this, it is found that atomic lattice fringes decreases with increasing Pd ratio in all prepared catalysts. To illustrate, the atomic lattice fringe of catalyst Ib was calculated to be 0.220 nm while it was calculated as 0.216 nm for catalyst IIIa as shown in Figure 13 (b).

a)

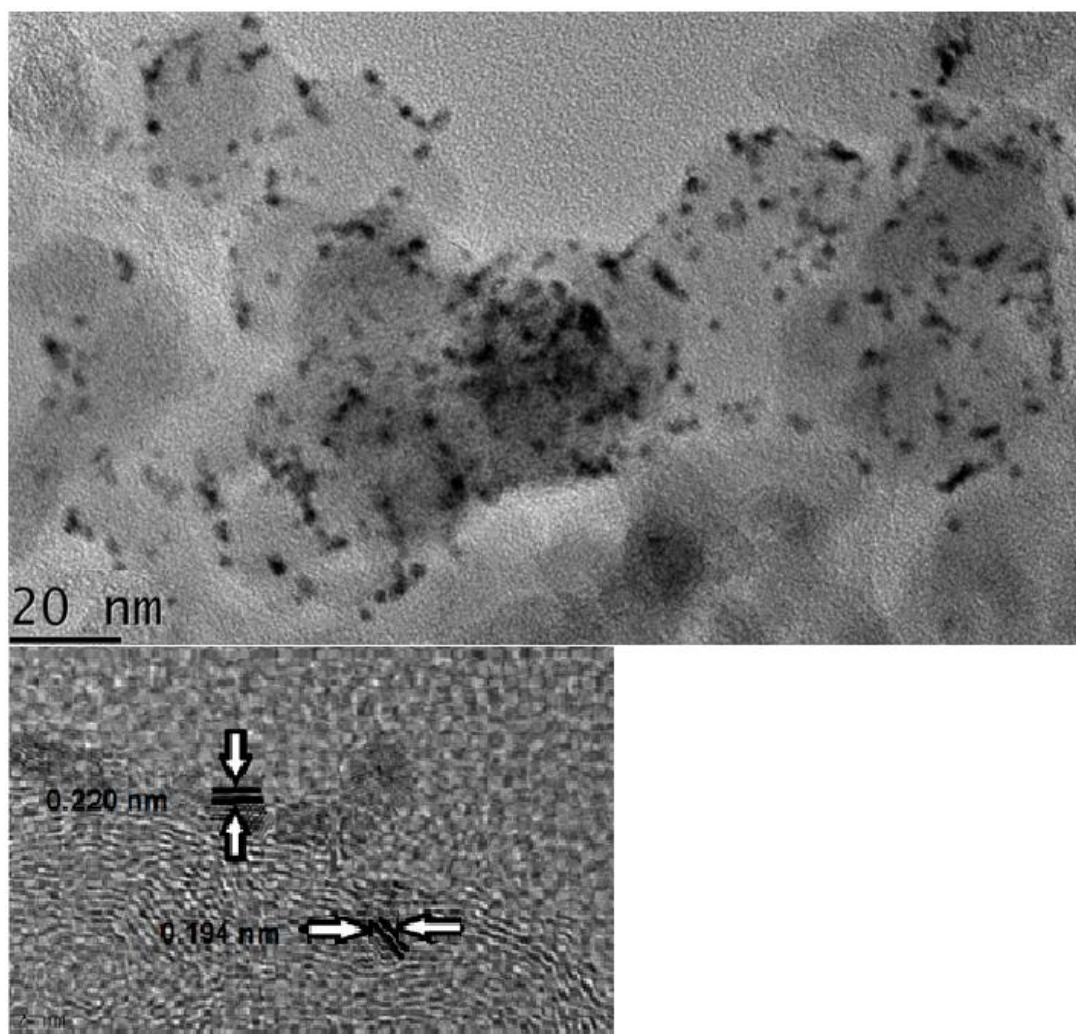


Figure 13. a) Transmission electron micrograph of catalysts Ia.

b)

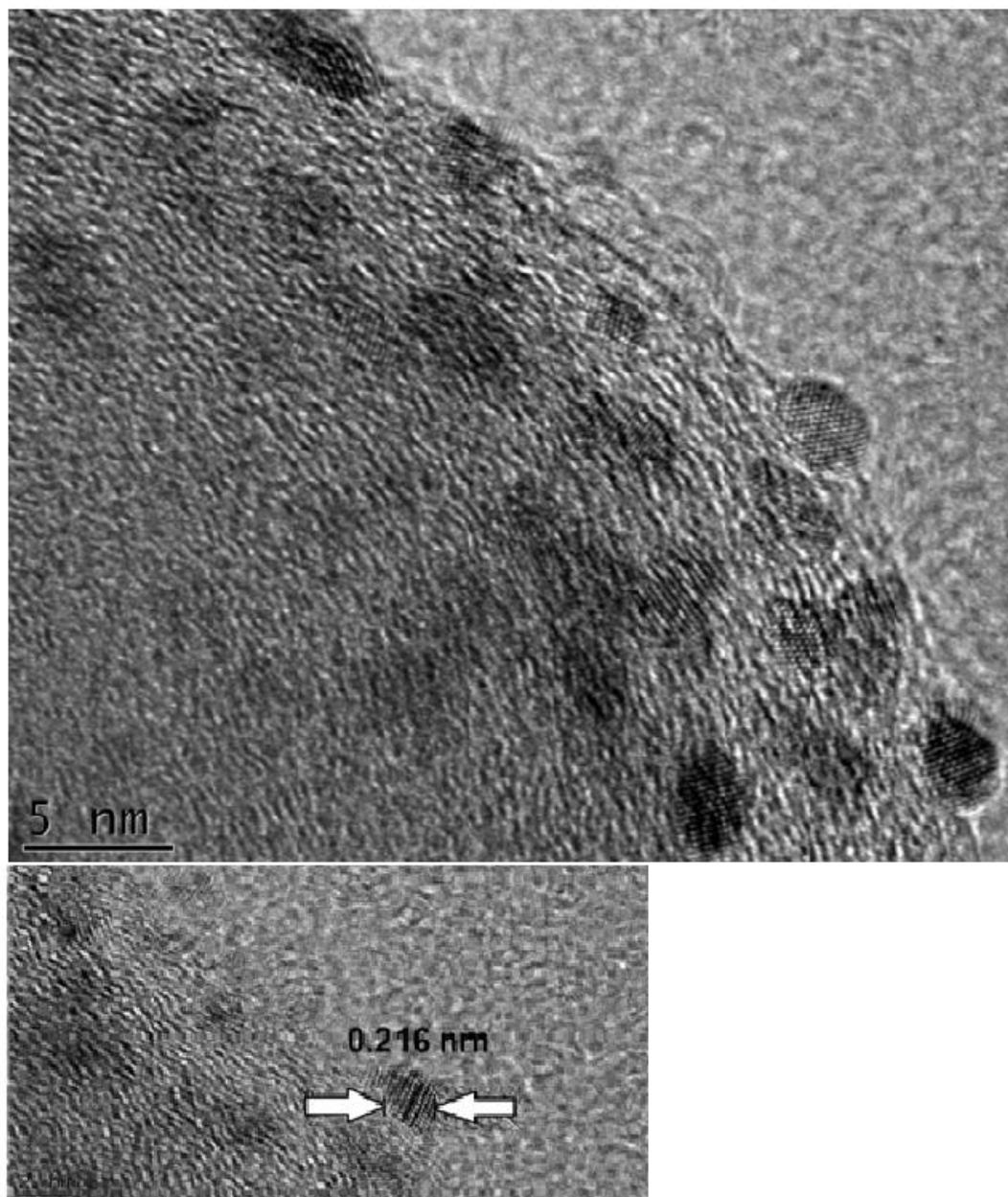


Figure 13. b) Transmission electron micrograph of catalyst IIIa.

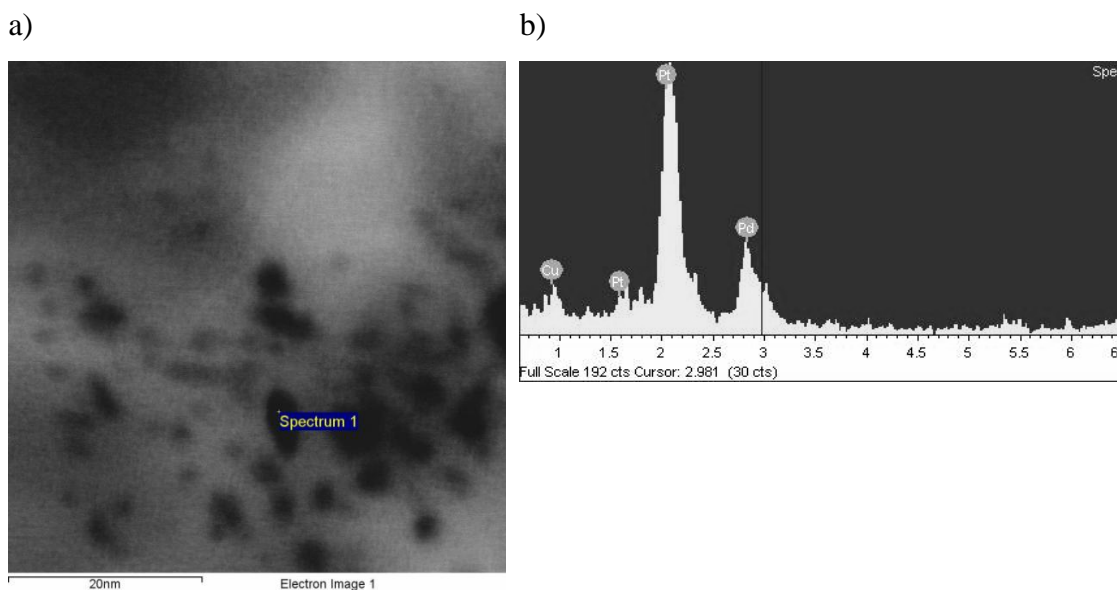


Figure 14. a) Transmission electron micrograph and b) EDS results for the spectrum 1 region of catalyst Ib

Transmission electron microscopy with energy dispersive X-ray spectroscopy analysis (EDS) of catalyst Ia and Ib, both in point and region analysis, showed that platinum and palladium are present in the expected atomic ratios. For instance, EDS results of these catalysts revealed the atomic ratio as ~ 90 % Pt and ~ 10 % Pd which are in good agreement with the nominal atomic ratios (for catalyst Ib, TEM micrograph and EDS results were given in Figure 14). For catalyst IIIa and IIIb, 70 % of the used Pd incorporated into the Pt, on the other hand, the remaining 30 % of the Pd did not incorporate according to the XRD data. Actually, these results were confirmed by EDS results since at some regions, the ratio of Pt/Pd was as expected while Pd existed richer in some other regions indicating low extent of alloying.

3.2. X-RAY PHOTOELECTRON SPECTROSCOPY

The chemical composition and the oxidation state of the metal nanoparticles was investigated by X-ray photoelectron spectroscopy (XPS). Gaussian-Lorentzian method was benefited for the fitting of all XPS peaks after background subtraction using Shirley's method. Moreover, all XPS peaks were analyzed in terms of relative peak area, chemical shifts of Pd and Pt peaks. It should also be stated that C 1s peak was chosen as a reference for the correction of the charging effects.

Figure 15 demonstrates the Pt 4f regions of all catalysts and as it is shown in the figure, Pt 4f regions can be separated into two doublets with the spin orbit splitting of 3.33 eV and with an intensity ratio of ca. 3:4. The first doublet of the platinum specie (Pt 4f_{7/2} at ~ 71.0 and 74.2 eV) can be attributed to Pt (0) while the second doublet of the platinum specie (Pt 4f_{5/2} ~74.6 and 77.8 eV) can be assigned to the Pt (IV) on the surface.³⁷

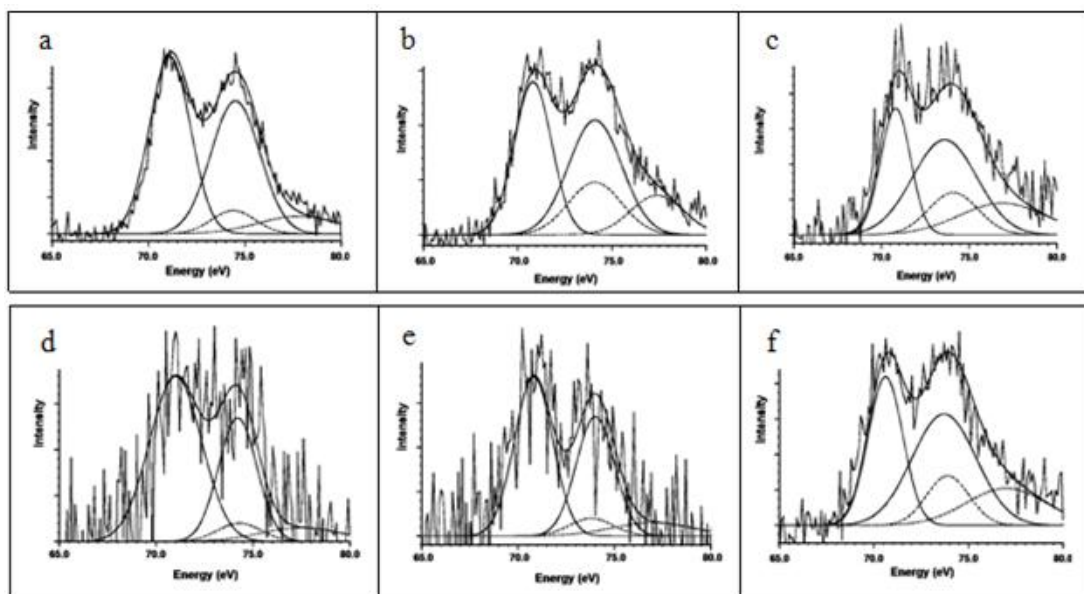


Figure 15. Pt 4f electron spectra of catalyst Ia (a), IIa (b), IIIa (c), Ib (d), IIb (e) and IIIb (f).

For the palladium case which is shown in Figure 16, Pd 3d region could be separated into two components with spin orbit splitting of 5.33 eV that is to assign presence of two different Pd species. The binding energies of about 335.2 eV which can be assigned as metallic Pd and about 337.9 eV which can be attributed as Pd²⁺ such as oxides or hydroxides.^{38,39} The relative intensities of those two peaks indicated that Pd⁰ was the principle oxidation state on the surface of all catalysts. The XPS results of all prepared Pt-Pd catalysts and their relative integrated intensities were given in Table 4.

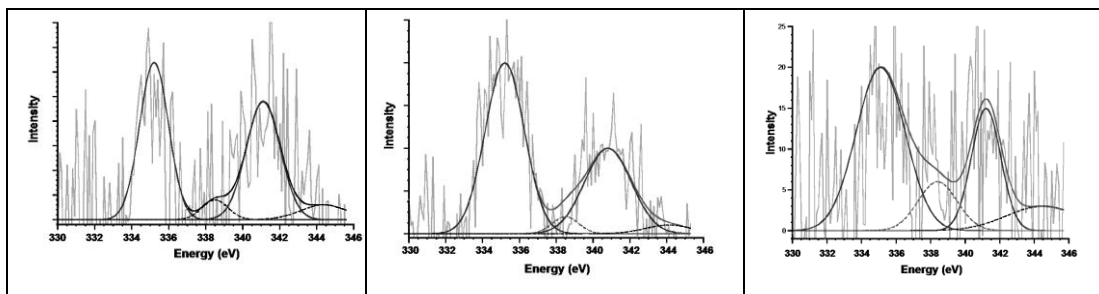


Figure 16. Pd 3d _{3/2} electron spectra of catalyst Ia (a), Ib (b), IIa (c)

It should be taken into consideration that higher electrochemical active area and catalytic activity toward methanol and ethanol oxidation reactions are due to the higher relative intensities of Pt (0) / Pt (IV) and Pd (0) / Pd (II). To illustrate, catalyst Ib and Ia have higher catalytic activities than that of the other prepared catalysts owing to the fact that catalyst Ib and Ia have extraordinarily higher Pt (0) to Pt (IV) and Pd (0) to Pd (II) ratios. Catalyst Ia-b < catalyst IIa-b < catalyst IIIa-b order represents the trend of the amount of Pd used in all catalysts. Also, this trend is valid for the amount of palladium that was not incorporated into Pt fcc structure and this gives rise to the higher presence of Pd²⁺ over the surface of the catalysts. Low extent of alloying with respect to the Pd amount used and low catalytic activity stems from

the increase in the amount of Pd (II) on the surface of the catalysts. Among the all catalysts; a shift toward higher binding energies for the Pt 4f peaks was observed for catalysts Ia and Ib and this is due to a decrease in the particle size as shown in Table 4. The integrated peak area ratios of Pt to Pd are also summarized in Table 4 and these results are in good agreement with XRD and TEM results.

Table 4. Pt 4f_{7/2} and Pd 3d_{3/2} Core Binding Energies, eV, for Pt-Pd catalysts (The numbers in parentheses are the relative percent intensities of the species.).

| Catalysts | Pt (0) | Pt (IV) | Pt(0)/ Pt(IV) | Pd (0) | Pd (II) | Pd(0)/ Pd(II) | Pt/ Pd ^a |
|-----------------|-------------|-------------|------------------|--------------|--------------|------------------|------------------------|
| Ia | 71.1 (85.1) | 74.5 (14.9) | 5.67 | 335.3 (88.1) | 338.1 (11.9) | 7.40 | 8.6 |
| IIa | 71.0 (72.4) | 74.2 (27.6) | 2.62 | 335.1 (78.2) | 338.1 (21.8) | 3.59 | 4.1 |
| IIIa | 70.9 (67.2) | 73.8 (32.8) | 2.05 | 335.0 (68.4) | 337.8 (31.6) | 2.16 | 2.5 |
| Pt/C (a) | 71.2 (71) | 74.4 (29) | 2.45 | | | | |
| Ib | 71.0 (87.4) | 74.2 (12.6) | 6.94 | 335.2 (93.2) | 338.1 (6.8) | 13.7 | 8.9 |
| IIb | 70.8 (83.9) | 74.0 (16.1) | 5.25 | 335.1 (84.4) | 337.7 (15.6) | 5.41 | 4.3 |
| IIIb | 70.7 (70.7) | 73.8 (29.3) | 2.41 | 335.0 (73.6) | 337.6 (26.4) | 2.79 | 2.9 |
| Pt/C (b) | 71.0 (76) | 74.4 (24) | 3.16 | | | | |

^a Integrated peak area ratios of Pt and Pd in XPS.

3.3. CYCLIC VOLTAMMETRY AND CHRONOAMPEROMETRY

The typical hydrogen and oxygen adsorption/desorption regions appear for the cyclic voltammograms of the prepared catalysts in 0.1 M HClO₄ at room temperature with a scan rate of 50 mV/s, Figure 17. Although small shifts were observed in the position of peaks, the cyclic voltammograms of all prepared catalysts are similar.

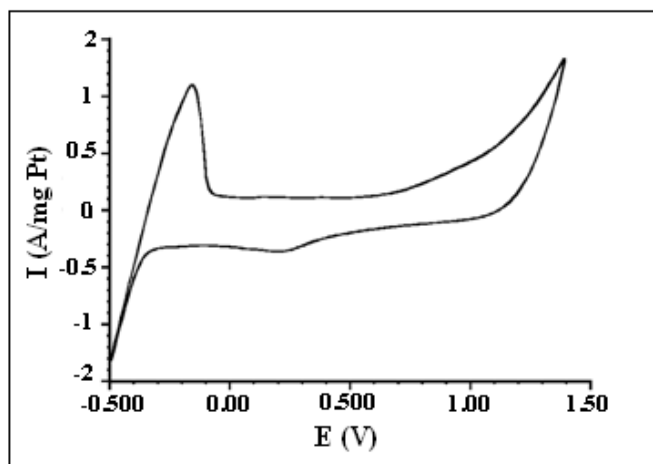


Figure 17. Cyclic voltammogram of catalyst Ib in 0.1 M HClO₄.

The addition of methanol to HClO₄ electrolyte resulted in a dramatic change in the appearances of the cyclic voltammograms and the recorded cyclic voltammograms exhibited a typical methanol oxidation reaction. A representative example of cyclic voltammogram for catalysts Ib is given in Figure 18.

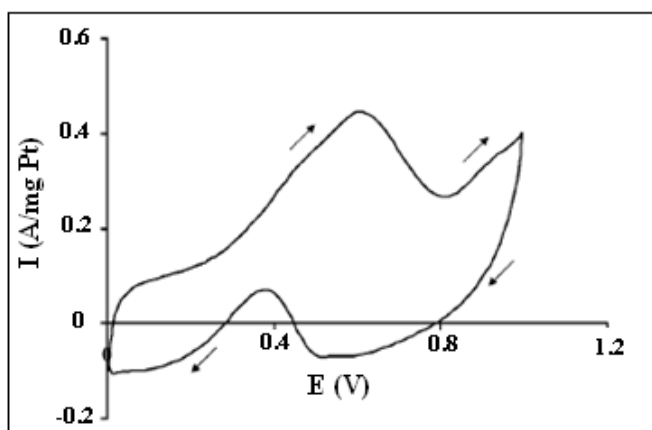


Figure 18. Cyclic voltammogram of catalyst Ib in 0.1 M HClO₄ + 0.5 M CH₃OH at room temperature with a scan rate of 50 mV/s.

Another dramatic change in the appearances of the cyclic voltammograms was observed due to the addition of ethanol to HClO_4 electrolyte and the cyclic voltammogram for catalyst Ib is given in Figure 19. Typical ethanol oxidation reaction is observed for the recorded cyclic voltammograms of all catalysts.

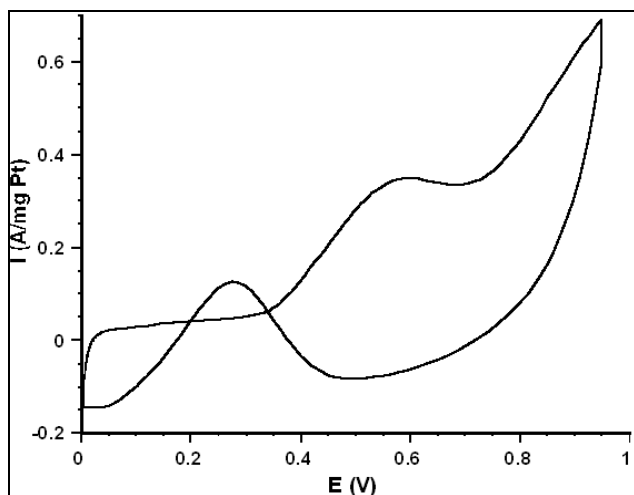


Figure 19. Cyclic voltammogram of catalyst Ib in 0.1 M HClO_4 + 0.5 M $\text{CH}_3\text{CH}_2\text{OH}$ at room temperature with a scan rate of 50 mV/s.

Figure 20, 21, 22 and 23 illustrate the comparisons of anodic parts of the cyclic voltammograms of all catalysts towards methanol and ethanol electrooxidation reactions. 1.2 times higher catalytic activity was observed for group “b” catalysts, which were stabilized by a branched surfactant, compared to the group “a” catalysts, which were stabilized by a linear surfactant. Among the all catalysts, catalyst Ib was found to be the most active catalyst with a catalytic activity of ~ 0.450 A / mg Pt at 0.57 V and ~ 0.350 A / mg Pt at 0.56 V for methanol and ethanol oxidation reactions respectively. Also, the catalytic activity of catalyst Ib is approximately 1.8 times higher than the Pt/C (b)¹⁸ which has catalytic activity of ~ 0.260 A / mg Pt at 0.65 V

for methanol and ~ 0.190 A / mg Pt at 0.73 V for ethanol oxidation reactions which are given in Table 3.3. In order to examine the enhancement in the catalytic activity, catalyst Ib was also compared with the commercial catalyst E-TEK (40 % Pt/Vulcan XC-72, ~ 90 A/g Pt and 25 A/g Pt catalytic activity for methanol and ethanol oxidation, respectively) and enhancement in the catalytic activity is approximately 5.0 and 14.0 times greater towards methanol and ethanol oxidation, respectively.

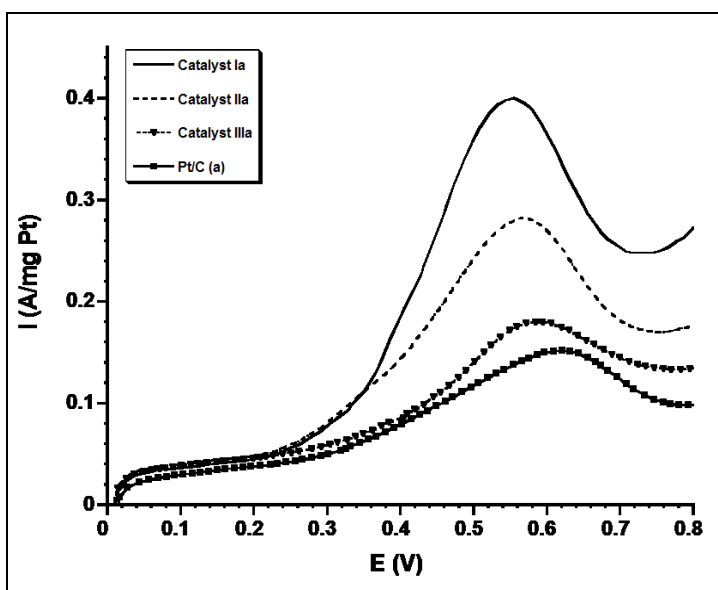


Figure 20. Anodic part of the cyclic voltammogram of catalysts Ia, IIa, IIIa and Pt/ C in 0.1 M HClO₄ + 0.5 M CH₃OH at room temperature. Scan rate is 50 mV/s.

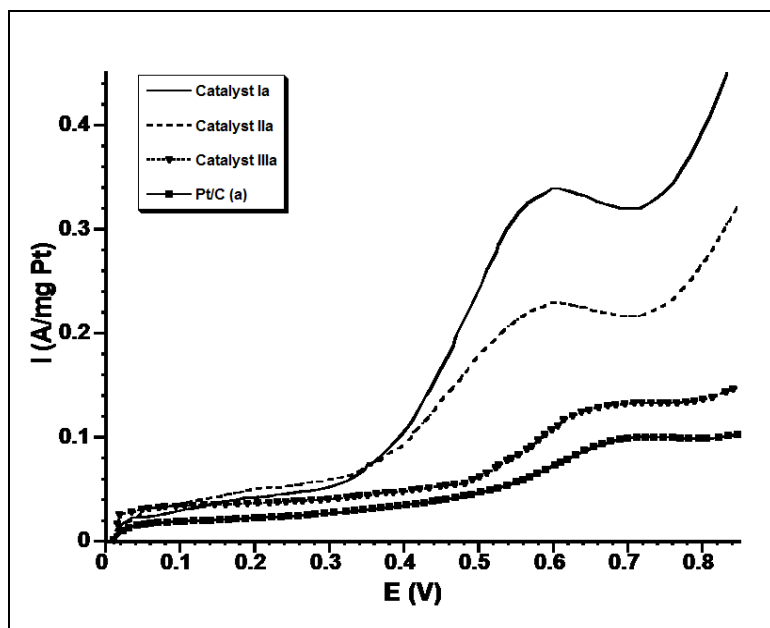


Figure 21. Anodic part of the cyclic voltammogram of catalysts Ia, IIa, IIIa and Pt/ C in 0.1 M HClO₄ + 0.5 M CH₃CH₂OH at room temperature. Scan rate is 50 mV/s.

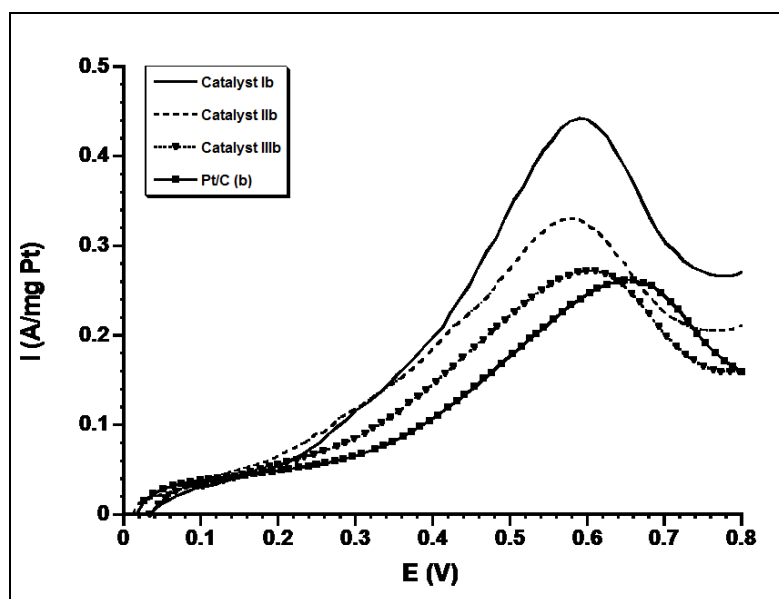


Figure 22. Anodic part of the cyclic voltammogram of catalysts Ib, IIb, IIIb and Pt/ C in 0.1 M HClO₄ + 0.5 M CH₃OH at room temperature. Scan rate is 50 mV/s.

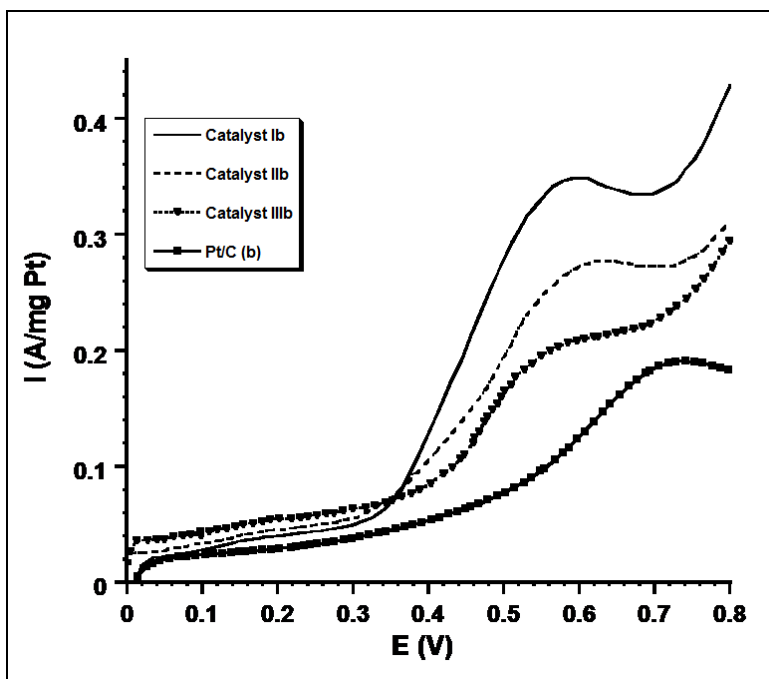
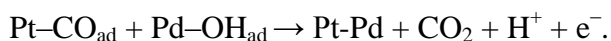
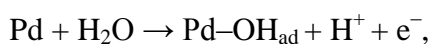
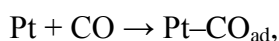


Figure 23. Anodic part of the cyclic voltammogram of catalysts Ib, IIb, IIIb and Pt/C in 0.1 M HClO₄ + 0.5 M CH₃CH₂OH at room temperature. Scan rate is 50 mV/s.

The two most active catalysts, catalyst Ia and Ib, possess the highest extent of alloying in terms of the palladium amount used which are 87.3 % and 89.0 %, respectively and the corresponding atomic ratio was 90 % Pt + 10% Pd. The percent insertion of Pd into Pt ranged from 15 % to 25 % for catalysts IIa-b and IIIa-b when the entire amount was taken into consideration. This illustrates that the Pd incorporated into Pt fcc was 70-80 %, in other words, the rest of the palladium existed as unincorporated in the catalyst which accounts for the inactiveness of the 20%-30% of the catalyst owing to the fact that oxidation reaction of alcohols does not take place on the unincorporated Pd. Hence, for catalysts IIa-b and catalyst IIIa-b, a decrease is to be expected in their catalytic activities.

The bifunctional mechanism which demonstrates the oxidation of adsorbed CO species by OH species can be used to explain the high CO tolerance of the Pt-Pd

catalysts which accounts for the improvement in the activity towards methanol electrooxidation reactions.⁴⁰ In addition to this, although bulk Pt and Pd have similar characteristics such as the coverage by OH species in the same potential range, oxidation of Pd takes place slightly easier than Pt. Moreover, in an acidic medium palladium was totally inactive for methanol and ethanol electrooxidation reactions. However, presence of palladium has a synergistic effect which causes Pt to have a change in the electronic density, weakening the Pt-CO bond and causing an improvement of the overall reaction by decreasing electrode poisoning.



Plot of oxidation current versus time (Chronoamperometry (CA)) was used to observe the long-term stability of all prepared catalysts under the same conditions. Figure 24 and 25 demonstrate the CA curves for methanol oxidation for group ‘a’ and ‘b’ catalysts, respectively, at the potential of 0.5 V (versus SCE). A similar trend, for a current decay in time can be observed for all catalysts and the results are approximately 0.026, 0.040, 0.019, 0.023, 0.012, 0.013, 0.005 and 0.009A (for 1 mg Pt) for catalysts Ia, Ib, IIa, IIb, IIIa, IIIb, Pt/C (a) and Pt/C (b), respectively for methanol oxidation reactions after a decay of 3600 s.

Double layer charge and the great number of active points on the catalysts for methanol oxidation reaction can be held responsible for the observed high initial current. The most active catalyst, catalysts Ib, was found to have a current that is approximately 4.4 times greater than the catalyst, Pt/C (b), after a decay of 3600s. The results of the chronoamperometry study are in harmony with those obtained from cyclic voltammetry study. To conclude, group “b” catalysts have not only higher stability but also higher poisoning tolerance when compared with group “a” catalysts for both methanol and ethanol oxidation reactions.

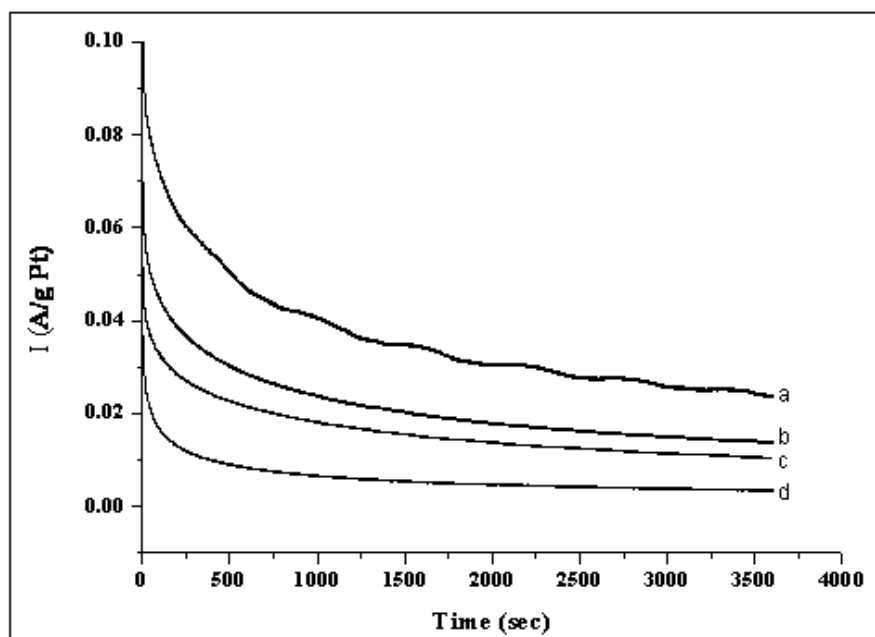


Figure 24. Chronoamperometric curves of methanol oxidation on catalyst Ia (a), IIa (b), IIIa (c) and Pt/C(a) (d) at 0.5 V (vs. SCE) in 0.1 M HClO₄ + 0.5 M CH₃OH.

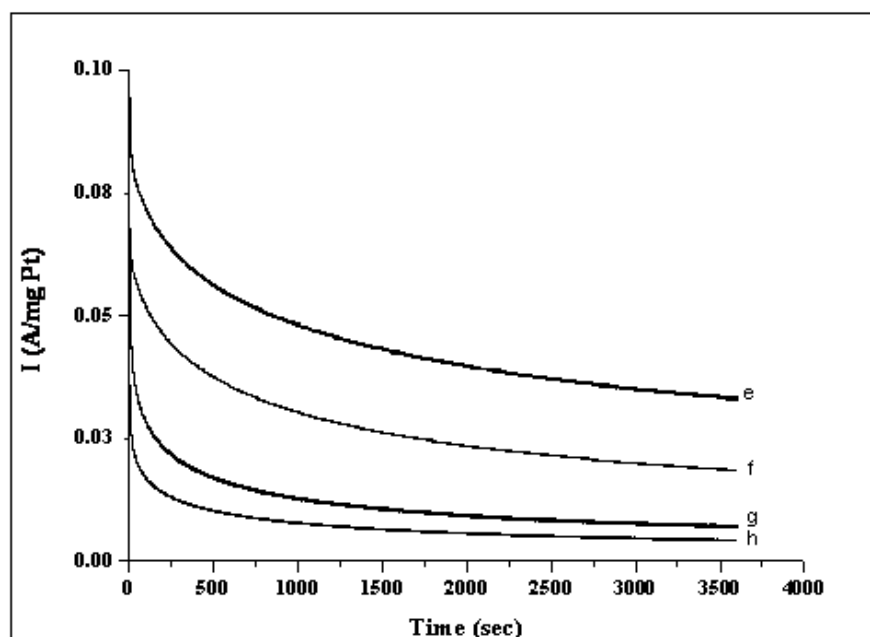


Figure 25. Chronoamperometric curves of methanol oxidation on catalyst Ib (e), IIb (f), IIIb (g) and Pt/C(b) (h) at 0.5 V (vs. SCE) in 0.1 M HClO₄ + 0.5 M CH₃OH.

In order to define the performance of the catalysts, I_f/I_b ratio can be used where I_f and I_b are the currents in the forward scan and in the reverse scan, respectively as illustrated in Figure 18. The higher the I_f/I_b ratio, the better the alcohol oxidation would be that is observed owing to the low accumulation of intermediate species on the surface of the catalysts for methanol and ethanol oxidation reactions.

In the light of the I_f/I_b ratios given in the Table 5, it can be stated that all Pt-Pd catalysts have higher I_f/I_b ratios than Pt/C (a & b) and the best performance is possessed by catalyst Ib. The reason why catalyst Ib is found to be the most active catalyst can also be explained by the higher I_f/I_b ratio of this catalyst indicating lower degree of poisoning. Table 5 gives maximum current, I_f/I_b ratios, onset and anodic peak potentials of all catalysts for methanol and ethanol oxidation reactions. As it is shown in the Table 5, Pt-Pd catalysts have lower onset and anodic peak potentials than those of Pt/C (a & b) catalysts¹⁶. Catalyst Ib comes into prominence again due to the possession of lower onset and anodic potentials among all catalysts which can also be a sign of the higher catalytic activity observed towards methanol and ethanol oxidation reactions.

Table 5. The onset and anodic peak potential, I_f/I_b ratios for all prepared catalysts in MeOH and EtOH.

| Catalysts | in MeOH | | | | in EtOH | | | |
|-----------------|----------------------|-----------|-----------------|-----------|----------------------|-----------|-----------------|-----------|
| | Max Current (A/mgPt) | Onset (V) | Anodic Peak (V) | I_f/I_b | Max Current (A/mgPt) | Onset (V) | Anodic Peak (V) | I_f/I_b |
| Ia | 0.40 | 0.26 | 0.55 | 7.54 | 0.34 | 0.32 | 0.56 | 3.39 |
| IIa | 0.28 | 0.26 | 0.56 | 4.97 | 0.22 | 0.34 | 0.57 | 2.25 |
| IIIa | 0.19 | 0.30 | 0.59 | 3.18 | 0.13 | 0.48 | 0.66 | 2.87 |
| Pt/C (a) | 0.16 | 0.30 | 0.62 | 2.30 | 0.10 | 0.50 | 0.69 | 2.19 |
| Ib | 0.45 | 0.19 | 0.57 | 18.8 | 0.35 | 0.33 | 0.56 | 3.67 |
| IIb | 0.33 | 0.21 | 0.57 | 5.63 | 0.28 | 0.34 | 0.58 | 2.32 |
| IIIb | 0.27 | 0.22 | 0.58 | 4.09 | 0.21 | 0.42 | 0.55 | 3.03 |
| Pt/C (b) | 0.26 | 0.28 | 0.65 | 3.80 | 0.19 | 0.50 | 0.73 | 1.06 |

As mentioned in the earlier part of this section, typical hydrogen and oxygen adsorption/desorption regions appeared in the cyclic voltammograms of the prepared catalysts in acidic medium and was given in Figure 17. The cyclic voltammogram in acid solution was used to calculate electrochemical surface area (ECSA) by the following equation⁴¹ and the results are summarized in Table 6 :

$$ECSA = \frac{Q_H}{[Pt] \times 0.21} \quad (3)$$

where Q is the electrical charge for hydrogen desorption, 0.21 mC/cm² is the Pt crystalline activity surface area transition constant and [Pt] (mg/cm²) is the Pt

loading. The chemical surface areas (CSA) of the prepared catalysts were calculated by using following equation³³;

$$CSA = \frac{6000}{\rho_{Pt-Pd} d} \quad (4)$$

$$\rho_{Pt-Pd} = X_{Pt} \cdot \rho_{Pt} + X_{Pd} \cdot \rho_{Pd}$$

where;

d = the crystalline particle diameter in Å (from the XRD results)

ρ_{Pt} = 21.40 g/cm³ (the density of Pt metal)

ρ_{Pd} = 12.02 g/cm³ (the density of Pd metal)

ρ_{Pt-Pd} = the density of Pt-Pd alloy

X_{Pt} = the atomic percent of Pt

X_{Pd} = the atomic percent of Pd.

The % catalyst utility which is the ratio of ECSA to CSA was calculated for each catalyst and Table 3.4. summarizes the particles size, CSA, ECSA and ECSA/CSA (% catalyst utility) for all catalysts. The observed trend in the % catalyst utility for group “a” and “b” catalysts is Pt/C (a) < catalyst IIIa < catalyst IIa < catalyst Ia and Pt/C (b) < catalyst IIIb < catalyst IIb < catalyst Ib, respectively. The observed trend is consistent with the catalytic activity since the greater the percent catalyst utility, that is to say, the greater the catalyst utilization area, the higher the catalytic activity is to be. The trend is also congruent with the results of XRD in view of the fact that catalytic activities of the catalysts increase as the Pd insertion into the Pt fcc structure (with respect to the amount of Pd used) ECSA and % catalyst utility increase.

Table 6. The comparisons of particle size, ECSA, CSA and ECSA/CSA (% catalyst utility) for all catalysts.

| Catalysts | Particle Size (nm) | CSA (m²/g) | ECSA (m²/g) | (ECSA/CSA)*100 (% catalyst utility) |
|------------------|---------------------------|------------------------------|-------------------------------|---|
| Ia | 3.00 ± 0.05 | 97.7 | 72.8 | 74.5 |
| IIa | 3.20 ± 0.07 | 96.0 | 63.3 | 65.9 |
| IIIa | 3.50 ± 0.09 | 92.2 | 52.2 | 56.6 |
| Pt/C (a) | 2.00 ± 0.04 | 140.2 | 42.5 | 30.3 |
| Ib | 3.20 ± 0.08 | 91.6 | 80.2 | 87.5 |
| IIb | 3.40 ± 0.11 | 90.4 | 62.1 | 68.7 |
| IIIb | 3.70 ± 0.14 | 87.2 | 56.2 | 64.4 |
| Pt/C (b) | 3.00 ± 0.07 | 93.4 | 44.4 | 47.5 |

CHAPTER 4

CONCLUSIONS

Two groups Pt-Pd nanoparticles were synthesized and characterized with the purpose of use as catalysts for the electrooxidation reactions of methanol and ethanol in order to explore the effect of Pd as a second metal on the catalytic activity. In addition to this, two different surfactants, 1- hexanethiol and 1,1 dimethyl hexanethiol were utilized, for group “a” and group “b” catalysts, respectively, as stabilizing agents in order to investigate the effect of surfactant on the particle size and the catalytic activity. The results were discussed in Chapter 3 in a detailed way and to conclude;

- The structure of the used surfactant has an effect on the size and the catalytic activities of Pt-Pd nanoparticles. For example, the usage of branched surfactant, 1,1 dimethyl hexanethiol, resulted in larger metal particle size formation and higher current density (group “b” catalysts) compared to those of linear surfactant, 1-hexanethiol (group “a” catalysts).
- TEM results revealed the uniform distribution of catalysts on carbon support with a narrow size distribution in the range of 3.0 to 3.7 nm.
- In terms of catalytic activity, group “b” catalysts were found to have greater catalytic activities than that of group “a” catalysts. In addition to this, catalyst Ib comes into prominence for being the most active catalyst among all for the electrooxidation reactions of methanol and ethanol owing to the superior characteristics that it owns such as highest extent of alloying (with respect to

the palladium amount used), higher active surface area (higher % catalyst utility), higher CO-tolerance and stability, higher Pt (0) to Pt (IV) and Pd (0) to Pd (II) ratios.

- Catalytic activity of the Pt-Pd binary catalysts towards methanol oxidation was found to be higher than the ethanol oxidation reactions presumably due to need of dissociative chemisorptions of ethanol molecule during electrooxidation process in which adsorption of strongly adsorbed (e.g. CO) and other oxidation reaction intermediates (e.g. acetaldehyde and acetic acid) may take place.

REFERENCES

- ¹ Bagotsky, V.S., *Fuel Cells: Problems and Solutions*, John Wiley & Sons, Inc., New Jersey, 2009.
- ² Davytyan, O.K., *The Problem of the Direct Conversion of the Chemical Energy of Fuels into Electrical Energy*, Publishing House of the USSR Academy of Sciences, Moscow, 1947.
- ³ Hoogers, G., Section I, *Fuel Cell Technology Handbook*, CRS Press LLC, Florida, 2003.
- ⁴ O'Hayre, R., Cha, S-W., Colella, W., Prinz, F.B., *Fuel Cell Fundamentals, 2nd Ed.*, John Wiley & Sons, Inc., New York, 2009.
- ⁵ Sen, S., Activity of Carbon Supported Platinum Nanoparticles Toward Methanol Oxidation Reactions: Role of Metal Precursor and New Surfactants, METU, Ankara, 2008.
- ⁶ Arico, A.S., Baglio, V., Antonucci, V., *Direct Methanol Fuel Cells*, Nova Science Publishers, Inc., New York, 2010.
- ⁷ Rapid Prototyping Laboratory at Stanford University, www-rpl.stanford.edu/research/energy/micro-fuel-cell/dmfc/, last update date: 15.12.2010.
- ⁸ Pramanik, H., Basu, S., *the Canadian Journal of Chemical Engineering*, 85, 781-85, 2007.
- ⁹ Lamy, C., Coutanceau C., Leger, J-M., *Catalysis for Sustainable Energy Production*, WILEY-VCH Verlag GmbH & Co., Weinheim, 2009.
- ¹⁰ Zhou, W., Zhou, Z., Song, S., Li, W., Sun, G., Tsiakaras, P., Xin Q., *Applied Catalysis B: Environmental*, 46, 273–285, 2003.
- ¹¹ Hamnett, A., *Catalysis Today*, 38, 445-457, 1997.
- ¹² Beden, B., Kadirgan, F., Lamy, C., Léger, J-M., *J. Electroanal. Chem.* 127, 75-85, 1981.
- ¹³ Watanabe, M., Uchida, M., Motoo, A., *J. Electroanal. Chem.*, 229, 395-406, 1987.
- ¹⁴ Kadirgan, F., Beyhan, S., Atilan, T., *Int J Hydrogen Energy*, 34, 4312-20, 2009.

- ¹⁵ Garcia, A.C., Paganin, V.A., Ticianelli, E.A., *Electrochim. Acta* 53, 4309–4315, 2008.
- ¹⁶ Yee, C. K., Jordan, R., Ulman, A., White, H., King, A., Rafailovich, M., Sokolov, J., *Langmuir*, 15, 3486-91, 1999.
- ¹⁷ Brust, M., Walker, M., Bethell, D., Schiffrin, D. J., Whyman, R., *J. Chem. Soc.*, 7, 801-2, 1994.
- ¹⁸ Sen, F., Gokagac, G., *J Phys Chem C*, 111-3, 1467-73, 2007.
- ¹⁹ Settle, F.A., *Handbook of Instrumental Techniques for Analytical Chemistry*, Prentice-Hall, Inc., New Jersey, 1997.
- ²⁰ Scholz F., *Electroanalytical Methods*, Springer, 2nd Ed., Berlin, 2002.
- ²¹ Department of Chemistry, University of Illinois at Chicago, Instrumental Analysis, Cyclic Voltammetry-An Example of Voltaic Methods by Shippy, S., Lu, M-J., <http://www.chem.uic.edu/chem421/cv.PDF>, March, 2007.
- ²² Kissinger, P.T., Heineman, W.R., *Laboratory Techniques in Electroanalytical Chemistry*, 2nd Ed., Marcel Dekker, Inc., New York, 1996.
- ²³ Earlham College; Department of Chemistry, http://www.earlham.edu/~chem/chem341/c341_labs_web/cyclic_voltammetry.pdf, Last Revision: February 06., 2004.
- ²⁴ He, B.B., *Two-dimensional X-Ray Diffraction*, John Wiley & Sons, Inc., Hoboken, 2009.
- ²⁵ Warren, B.E., *X-Ray Diffraction*, Dover Publications, Inc., New York, 1990.
- ²⁶ The Science Education Research Center, Carleton College, Geochemical Instrumentation and Analysis; http://serc.carleton.edu/research_education/geochem_sheets/BraggsLaw.html, Lat modified: April 21, 2010.
- ²⁷ Carter, C.B., Williams, D.B., *Transmission Electron Microscopy A text Book for Materials Science*, Springer, 2009.
- ²⁸ Koninklijke Philips Electronics-Research; Transmission Electron Microscopy (TEM), <http://www.research.philip.com/technologies/matanalysis/downloads/7-temtn.pdf>, April, 2008.

- ²⁹ Watts, J.F., Wolstenholme, J., *An Introduction to Surface Analysis by XPS and AES*, John Wiley and Sons, Ltd., Chichester, 2003.
- ³⁰ Department of Chemistry, McGill University, XPS Theory by Paynter, R., http://csacs.mcgill.ca/francais/docs/CHEM634/XPS_Paynter_t.pdf, Last Date Accessed: December 17,2010.
- ³¹ (JCPDS-ICDD, Card No. 04-802).
- ³² He, C. Z., Kunz, H. R., Fenton, J. M., *J Electrochem Soc*, 144, 970–9, 1997.
- ³³ Wang, Z. B., Yin, G. P., Shi, P. F., *J. Electrochem. Soc.*, 152, A2406–A12, 2005.
- ³⁴ Li, H., Sun, G., Cao, L., Jiang, L., Xin, Q., *Electrochim. Acta*, 52, 6622-9, 2007.
- ³⁵ Klug, H., Alexander, L., *X-ray diffraction procedures, 1st Ed.*, John Wiley & Sons, Inc., New York, 1954.
- ³⁶ Yonezawa, T., Toshima, N., Wakai, C., Nakahara, M., Nishinaka, M., Tominaga, T., Nomura, H., *Coll. and Surf. A*, , 169, 35-45. 2000.
- ³⁷ Sen, F., Gokagac, G., *J. Phys. Chem. C*, 111 (15), 5715-20, 2007.
- ³⁸ Cordi, E. M., Falconer, L., *J. Cat.*, 162, 104-17, 1996.
- ³⁹ Kim S.K., Kim, T.W., Koh, H.L, Lee, S. H., Min, B. R., *Applied Cat. A*, General 280, 125-31, 2005.
- ⁴⁰ Watanabe, M., Motoo, S., *J. Electroanal. Chem*, 60, 275-83, 1975.
- ⁴¹ R.J. Woods, *Electroanal. Chem.*, 9,1, 1976.